Synthesis of Bi_2O_3/Sb_2S_3 nanocomposite for photocatalytic degradation of Rhodamine-B and Tetracycline

A Dissertation

Submitted for the partial fulfillment

of

the award of the degree of

MASTERS OF SCIENCE

In

CHEMISTRY

By

CHARU

(Reg. No. : 302102005)

Under the supervision of

DR. SOUMEN BASU

Professor

School of Chemistry and Biochemistry

Thapar Institute of Engineering and Technology

Patiala-147004 , Punjab

July 2023

CERTIFICATE

This is to certify that the dissertation entitled ***"Synthesis of Bi_2O_3/Sb_2S_3 nanocomposite for the photocatalytic degradation of Rhodamine-B and Tetracycline"*** being submitted by **Charu** to the **School of Chemistry and Biochemistry, Thapar Institute of Engineering and Technology, Patiala,** in partial fulfillment of the requirements for the award of the degree of **Master of Science in Chemistry,** is an authentic record of the work carried out by the candidate under my/our guidance and supervision. She has complied with all procedures for submitting this dissertation, which, as far as I know, meets the necessary standards.

There hasn't been any partial or complete submission of the dissertation's findings to another university or institute for the award of another degree or diploma.

Date: 21-07-23 **Charu**

Place: TIET, Patiala **(302102005)**

It is certified that the aforementioned statement made by the student is correct to the best of my/our knowledge and belief.

Dr. Soumen Basu

Professor

School of Chemistry and Biochemistry

Thapar Institute of Engineering and Technology, Patiala.

CANDIDATE'S DECLARATION

I hereby declare that the dissertation entitled ***"Synthesis of Bi_2O_3/Sb_2S_3 nanocomposite for the photocatalytic degradation of Rhodamine-B and Tetracycline"*** submitted in partial fulfillment of the requirements for the award of a degree in **Masters of Science in Chemistry** to the **School of Chemistry and Biochemistry at the Thapar Institute of Engineering and Technology, Patiala** is a record of my own work done under the supervision of **Dr. Soumen Basu**, Professor, School of Chemistry and Biochemistry, Thapar Institute of Engineering and Technology. Additionally, none of the components of this dissertation have been submitted to another university for consideration for a different degree or diploma.

Date : 21-07-23 **Charu**

Place: TIET, Patiala **(302102005)**

ACKNOWLEDGEMENT

First and foremost, I want to express my gratitude to **God** for providing me with the strength and determination that I needed throughout the entire duration of this project.

I extend my deepest and sincerest appreciation to my project supervisor, **Dr. Soumen Basu,** Professor, School of Chemistry and Biochemistry, Thapar Institute of Engineering and Technology, Patiala. His immense support, constant motivation, and invaluable guidance have been instrumental in the successful completion of my project. I am genuinely grateful for the privilege and honor of working under his constructive mentorship, which consistently steered me in the right direction.

I am immensely grateful to **Dr. Satnam Singh,** Professor, and Head of the School of Chemistry and Biochemistry, for granting me the invaluable opportunity to work on this dissertation project. I would like to express my heartfelt appreciation to all the faculty and staff at SCBC for their guidance and support throughout this journey.

I am deeply grateful to **Ms. Shelly** for her unwavering support, comprehensive understanding, and vast expertise. Her genuine sincerity, patience, and warm-hearted nature have been a constant source of inspiration. Her thoughtful suggestions, delivered with kindness and encouragement, have played a pivotal role in ensuring the smooth completion of this project.

I am filled with profound gratitude towards my lab seniors, **Dr. Neeraj, Mr. Pritam**, **Ms. Aayushi**, **Ms. Anushka, Mr. Ranjit Jha,** and **Mr. Padam** who consistently provided me with cooperative guidance, a friendly demeanor, and invaluable assistance throughout my project.

I express my obligation to the **Thapar Institute of Engineering and Technology & School of Chemistry and Biochemistry** for generous funding and the essential infrastructure and research facilities that enabled me to conduct my experiments successfully.

Lastly, but of utmost importance, I am immensely thankful to my **parents, family, and friends**, who have showered me with unconditional love, priceless affection, heartfelt prayers, and constant support in every facet of my life.

TABLE OF CONTENTS

LIST OF FIGURES

LIST OF TABLES

LIST OF SCHEMES

LIST OF ABBREVIATIONS

BO	Bi_2O_3
SBS	Sb_2S_3
BOSBS	Bi_2O_3/Sb_2S_3 nanocomposite
RhB	Rhodamine-B
TC	Tetracycline
XRD	X-Ray Diffraction
XPS	X-Ray photoelectron Spectroscopy

SEM	Scanning Electron Microscopy
TEM	Transmission Electron Microscopy
EDS	Energy-dispersive X-Ray Spectroscopy
PL	Photoluminescence Spectroscopy
BET	Brunauer–Emmett–Teller
UV-Vis	Ultraviolet-visible
DRS	Diffuse Reflectance Spectroscopy
TOC	Total organic carbon
COD	Chemical oxygen demand
FT-IR	Fourier Transform Infrared spectroscopy
TGA	Thermogravimetric analysis
eV	Electron Volt
λ_{max}	Absorption Maxima
wt.	Weight
m^2/g	Meter square per gram
nm	Nanometer
^{o}	Degree Celsius
mL	Milliliter
a.u.	Arbitrary Units
g/L	Gram per liter
h	Hours
min	Minutes
mg	Milligram
PCS	Porous carbon spheres

ABSTRACT

The application of photocatalytic decomposition has garnered significant interest as a viable approach to mitigate water contamination and environmental pollution. In the face of expanding industrial development and rapid population increase, water pollution poses a grave threat to the ecosystem and human well-being. This study employs a hydrothermal technique to synthesize the photocatalyst by varying the mole ratios of Bi_2O_3 and Sb_2S_3. Loading Sb_2S_3 onto Bi_2O_3 enables broad-spectrum solar light absorption, efficient segregation of charges, and enhanced surface area. The characteristics of the elements were thoroughly examined through XRD and XPS techniques, enabling analysis of the crystal structure, chemical valence, and surface chemical makeup. The formation of smaller Sb_2S_3 nano-rods, effectively deposited onto bigger Bi_2O_3 nano-rods, was visually confirmed via SEM and TEM images. The EDS spectra evidenced the even dispersion of elements. PL and UV–DRS spectroscopy provided evidence of low charge recombination and a narrow band gap, indicating appropriate traits for photocatalysis. Furthermore, BET analysis revealed the photocatalyst's extensive surface area and mesoporous nature. Remarkable decomposition efficiencies were achieved, with a 98.2% degradation rate (rate constant = 0.03149 min^{-1}) observed for Rhodamine-B and a 91.5% degradation rate (rate constant = 0.01749 min^{-1}) achieved for Tetracycline. These impressive results were obtained using 0.3 g/L of the 13BOSBS photocatalyst under sunlight illumination for 120 min. Reusability studies confirmed the catalyst's impressive stability, with approximately 74.4% degradation of Rh-B maintained even after seven consecutive runs. Scavenger experiments highlighted the crucial role of $^{\bullet}OH$ radicals in the photodecomposition mechanism. For the RhB dye, the 13BOSBS catalyst demonstrated remarkable 90.2% and 85% reductions in COD and TOC, respectively. The commercially available TC powder substantially reduced 84% in COD and 80% in TOC. Owing to its excellent attributes and simple synthesis method, the fabricated heterojunction holds great potential for ecosystem rehabilitation.

Keywords: Bi_2O_3/Sb_2S_3, Tetracycline, Rhodamine-B, Photocatalytic degradation, Wastewater.

CHAPTER 1 - INTRODUCTION

1.1 Basic frame

The escalating global energy requirements and the detrimental effects of environmental pollution have become the foremost priorities for humanity [1–3]. The severity of water contamination resulting from substances such as pesticides [4], phenolic compounds [5], dyes [6,7], microplastics [8], pharmaceutical compounds [9], and others has been widely acknowledged. These substances pose significant challenges due to their high toxicity, carcinogenic properties and resistance to degradation. Each year, a staggering amount of approximately 45,000 tons of organic dye is generated, and regrettably, over 11% of this quantity finds its way into our precious water bodies [10]. This hazardous and vividly colored waste degrades water quality and increases toxicity levels. In addition to dyes, contaminants from pharmaceutical industries, especially antibiotics, pose a grave and imminent environmental threat [11]. Pharmaceutical substances have been detected in wastewater reclamation plant effluents and superficial waters, starting from nanograms per liter (ng/L) and going upto micrograms per liter (μg/L) [12]. The environmental risk posed by these drugs' persistence in water bodies is severe. Hence, ensuring adequate treatment of wastewater prior to its discharge is of paramount importance in preserving the delicate balance of our ecosystem.

1.2 Rhodamine-B dye (RhB), a colored pollutant

Rhodamine-B (RhB) is solvable in aqueous medium. It is toxic, fluorescent and is extensively employed in the textile industry. With a pKa value of approximately 3.7, RhB is mostly found in its positively charged state (RhB^{+}) in water-based solutions. It's structure is mentioned in **Fig. 1.1.** However, upon surpassing the pKa threshold, the formation of a zwitterion ($RhB^{\pm}$) occurs due to the deprotonation of the carboxyl group [13]. RhB holds great prominence in the food and fabric-making sectors and plays a vital function in coloring procedures within the leather, paint, pulp and paper industries [14]. However, exposure to RhB can result in severe allergic reactions affecting the eyes and skin, causing throat irritation, nausea, itching, and gastrointestinal problems. Furthermore, RhB causes mutagenic, neurotoxic, and reproductive side effects [15]. It's detrimental impact on human

beings necessitates it's urgent degradation to prevent water pollution and safeguard our well-being.

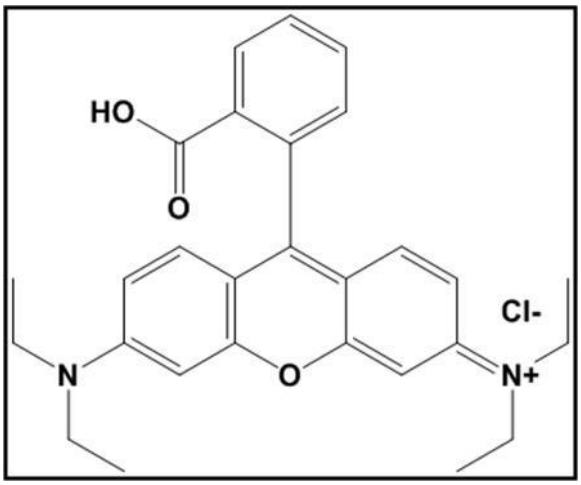

Fig. 1.1 Structure of Rhodamine-B dye.

1.3 Tetracycline (TC), a pharmaceutical contaminant

Tetracycline (TC) is a strong wide-spectrum antibiotic extensively employed in both veterinary and human medicine to address and mitigate various illnesses.

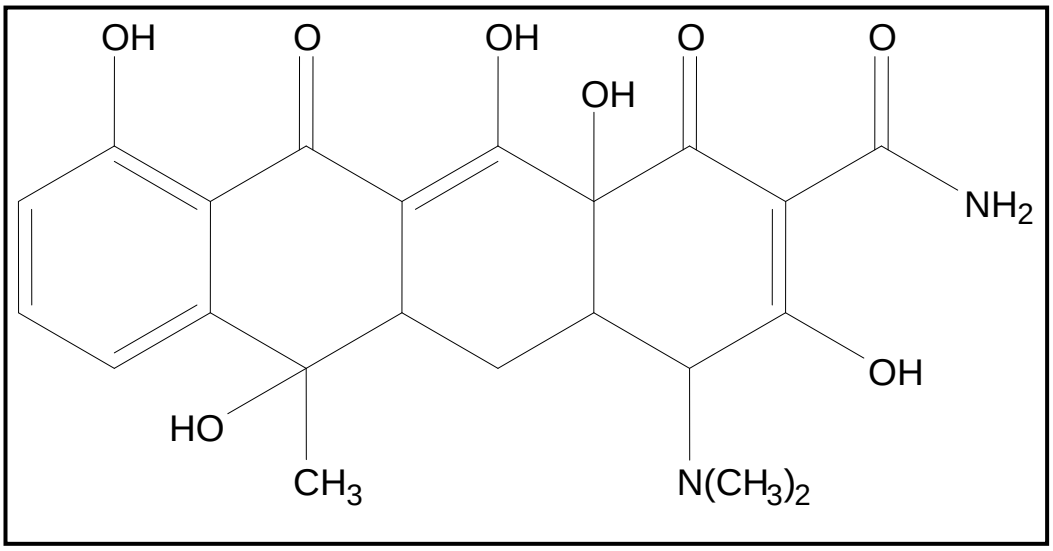

Fig. 1.2 Structure of Tetracycline antibiotic.

Its wide-ranging efficacy enables it to effectively suppress the growth of various micro-organisms, including bacterias with both kinds of stains (positive and negative) and protozoan parasites like chlamydia, mycoplasma and rickettsia [16]. Tetracycline's affordability and strong effectiveness have established it as a prevalent and frequently utilized antibiotic in medical practice. The structure of TC is shown in **Fig. 1.2.** However, TC is not effectively absorbed by the digestive systems of animals and humans, resulting in its

excretion through faeces or urine, typically accounting for 50-80% of the administered dose [17]. Environmental monitoring studies have revealed significant concentrations of TC (ranging from 100 to 500 mg/L) in the wastewater discharges of hospitals and pharmaceutical facilities. Furthermore, tetracycline poses risks to both drinking and irrigation water sources, and it also disrupts the microbial balance within the human intestinal flora. Its over consumption is highly fatal for the mankind [18].

1.4 Practices for wastewater treatment

It is crucially imperative to eliminate the detrimental and potentially life-threatening organic pollutants like dyes, microplastics, antibiotics, pesticides etc. Numerous approaches have been explored in an attempt to eradicate the persistent pollutants released into the aquatic environment. These processes include solvent extraction, reverse osmosis, sedimentation, adsorption, oxidative degradation, precipitation, and biological and electrochemical methods [19]. However, these techniques exhibit relatively slow progress, necessitate meticulous temperature and pressure control, and pose cost challenges. Moreover, these methods do not cause complete eradication of the pollutant but rather result in its conversion into secondary pollutants, which subsequently demand additional removal measures [20]. So, it is essential to embrace economically viable practices that ensure complete degradation of pollutants while also being environmental friendly. One such technique is photocatalysis which is explained ahead.

1.5 Photocatalysis and some heterojunction photocatalysts

Photocatalysis has emerged as a highly attractive and superior method for degrading dyes, antibiotics, present in water. It offers several advantages, including simplicity, innocous nature, prolonged durability, non-erosive properties, and cost-effectiveness [21]. Photocatalysis harnesses the power of sunlight, utilizing a solid photocatalyst to effectively eliminate organic pollutants. Moreover, through this process, harmful pollutants are entirely eliminated as they are transformed into simpler compounds such as carbon dioxide (CO_2) and water (H_2O) [22]. This elegant approach holds the enormous potential to address environmental challenges with remarkable effectiveness as shown in **Fig. 1.3.**

An exquisite array of metal oxides, phosphides, sulphides, and other compounds has gracefully emerged as semiconductors, adorning the field of photocatalytic degradation [22]. Among the vast collection, bismuth-based nanomaterials have emerged as captivating figures

within the realm of semiconductor-based photocatalysis. Among them, Bi_2O_3 (BO) stands out as a promising option owing to its narrow energy gap starting from ~2 eV and going upto 3.96 eV [23]. Also, it has a high refractive index and photoluminescence, non-toxicity, high photostability, abundant oxygen vacancies, and remarkable optical absorption properties These properties enable it to absorb broad range of visible light [24,25]. But, the pristine form of Bi_2O_3 encounters an obstacle due to the quick reunion of photogenerated charged particles (electrons and holes), smaller surface area, and the lower conduction band edge position [26]. However, the fusion of Bi_2O_3 with other semiconductor photocatalysts has emerged as an increasingly favored approach, as it engenders the formation of heterojunction photocatalysts. Their successful synthesis tends to lower the reassimilation of the charges, and increases the lifespan of photoinduced charges due to the synergistic effect of both semiconductors. α-Bi_2O_3/g-C_3N_4 heterojunction exhibited degradation efficiency of 80.5 % for doxycycline under the radiance of visible light [27]. About, 94% degradation of Tramadol was achieved with α-NiS/Bi_2O_3 photocatalyst [28].

Sb_2S_3 (SBS) is a remarkable photocatalyst owing to its exceptional characteristics. These include its small energy gap of ~1.84 eV, enabling it to harvest efficient sunlight. Notably, SBS exhibits non-carcinogenic properties and is economically viable, further enhancing its appeal as a viable option for photocatalytic applications [19]. Sb_2S_3, a significant semiconductor, possesses remarkable photoelectronic, electrochemical and optical characteristics. Hence, Sb_2S_3 nanomaterials hold enormous potential for a variety of uses, including gas sensors, photoelectronic devices, lithium-ion batteries, solar cells, near-infrared optical devices , and more [29]. About 89, and 64% of degradation efficiency was achieved for RhB, and thiamethoxam, respectively by Sb_2S_3/rGO photocatalyst. Sb_2S_3/PCS (porous carbon spheres) heterojunction possessed the degradation rate of 77.65% for RhB and 62% for thiamethoxam under visible light [13]. About 91.23% of degradation efficiency of methylene blue dye has been achieved by Sb_2S_3/α-Ag_2WO_4 heterojunction within 60 min. [30].

1.6 Present work

The present study focuses on synthesizing a novel nanocomposite Bi_2O_3/Sb_2S_3 (BOSBS) and its various mole ratios. While pristine BO and SBS have been previously synthesized and paired with various materials, but their combination with each other is a new and innovative approach explored in this work for the photocatalytic application. The synergy achieved

through the combination of Sb_2S_3 and Bi_2O_3 has shown significant potential in elevating the photocatalytic capabilities of Bi_2O_3. Heterojunction formation lowers the recombination rate of charge carriers, consequently leading to improved photocatalytic performance.

A hydrothermal approach was used in this investigation to fabricate various mole ratios of BOSBS nanocomposite. The synthesized photocatalyst was then evaluated for its performance for the degradation of a colored pollutant (RhB) and a colorless pollutant (TC) with the help of solarlight. A comprehensive set of experiments viz., the optimization of photocatalyst concentration, kinetic analysis, pH influence, reusability assessment, and scavenger studies were carried out. Furthermore, the performance of the fabricated photocatalysts was evaluated by checking their degrading power in comparison to that of the commercially available TiO_2-P25. Additionally, mineralization experiments were done to assess the photocatalysts' effectiveness.

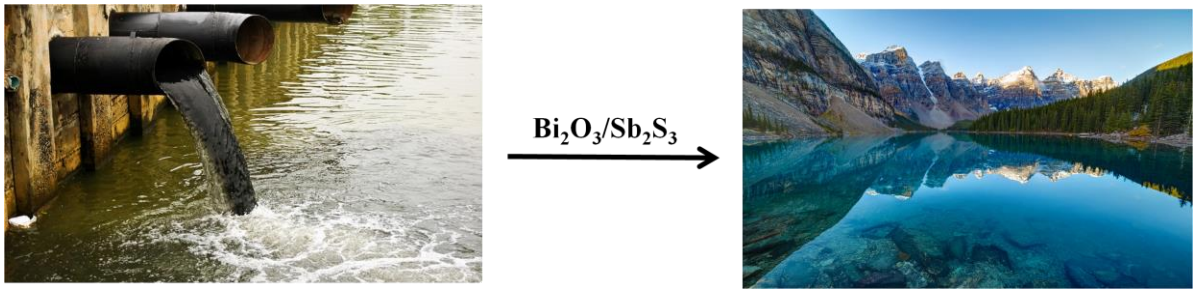

Fig. 1.3 Conversion of wastewater into clean water using BOSBS photocatalyst.

1.7 Thesis objectives

Our fundamental approach involved the synthesis of a nanocomposite that aimed at effectively eliminating and breaking down toxic pollutants present in wastewater. This was achieved by incorporating Sb_2S_3 onto Bi_2O_3, resulting in the formation of a highly efficient Bi_2O_3/Sb_2S_3 heterojunction nanocomposite for wastewater treatment.

The nanocomposite's structure and composition were meticulously analyzed using advanced techniques such as Brunauer–Emmett–Teller (BET) and X-ray Diffraction spectroscopy (XRD). The elemental oxidation state was thoroughly investigated through the application of X-ray photoelectron spectroscopy (XPS). To gain insight into its morphology, Transmission Electron Microscopy (TEM) and Scanning Electron Microscopy (SEM) were used, confirming its intricate form. Furthermore, Photoluminescence spectroscopy (PL) enabled a comprehensive assessment of the photocatalyst's electronic properties, providing valuable insights into its efficiency.

To comprehensively examine and compare the decomposition ability of the photocatalyst, a range of studies were conducted. These studies encompassed investigating the photocatalytic activity in both dark conditions and under sunlight exposure, with measurements taken at different time intervals. Additionally, the influence of different factors in the reaction that affects catalyst's effectiveness of decomposition was investigated. These parameters included catalyst concentration, the role of scavengers, impact of various light sources, reusability efficiency, specific pH ranges and more. By meticulously analyzing these factors, a deeper understanding of the photocatalyst's performance and its response to different conditions was attained.

In order to culminate, the aforementioned findings were gathered to substantiate the remarkable photocatalytic efficacy of the synthesized heterojunction photocatalyst.

CHAPTER 2 - LITERATURE REVIEW

In previous studies, researchers have successfully created a variety of nanocomposites using Bi_2O_3 and Sb_2S_3 as the primary materials. These hybrid nanocomposites exhibit different structures, surface shapes, and sizes. They have demonstrated great promise in various practical uses, such as breaking down harmful organic pollutants, detecting dangerous heavy metal ions, generating hydrogen, promoting nitrification, etc. Combining Bi_2O_3 and Sb_2S_3 in the nanocomposite demonstrates impressive efficiency in breaking down dyes and antibiotics. Adding Sb_2S_3 to the surface of Bi_2O_3 significantly enhances the separation of charged particles created by light, leading to broader light absorption and improved photocatalytic performance.

Berekute *et al.,* 2023 successfully created a novel binary nanocomposite P-g-C_3N_4/α-Bi_2O_3 using a hydrothermal-calcination technique. The nanocomposite of P-g-C_3N_4/α-Bi_2O_3 (25 wt%) demonstrated superior catalytic action compared to individual components for degrading 4-hydroxy benzophenone (4H-BP) and benzophenone-1 (BP-1). The creation of heterojunction and improved light absorption, which considerably improve the separation and transmission of charged particles generated through light, are principally responsible for the enhanced photocatalytic efficacy. This nanocomposite demonstrated high photocatalytic performance for BP-1 and 4H-BP, achieving 95% and 94% degradation under visible light conditions, respectively [31].

Kashmery *et al.,* 2023 successfully produced Bi_2O_3 with the help of a sol-gel procedure taking surfactant as a stabilizing agent. Through the synthesis of nanocomposites comprising Bi_2S_3/Bi_2O_3 with different Bi_2S_3 concentrations (ranging from 1.0% to 4.0% by weight), proficient photocatalysts for the degradation of Tetracycline under visible-light irradiation were successfully formulated. Through optimization, they found that a dose of 2.0 g/L for Bi_2S_3/Bi_2O_3 nanocomposite achieved rapid TC solution degradation. This photocatalyst completely removed the antibiotic after only 90 min of irradiation [32].

Subalakshmi *et al.,* 2022 fabricated $SrWO_4$/Bi_2O_3 nanocomposite through co-precipitation. They characterized it using techniques such as FT-IR, SEM, HR-TEM, UV-DRS, XRD, EDS, TGA, FT-IR, and Raman spectroscopy. The synthesized nanocomposite was tested for its ability to deteriorate methylene blue with the help of visible light. The highest efficiency

of 99% was achieved using $SrWO_4/Bi_2O_3$ (0.1 g/L), with 10mM starting amount of MB, and irradiation was done for 180 min. [33].

Pournemati *et al.,* 2022 designed $TiO_2/MgBi_2O_6/Bi_2O_3$ ternary visible-light-driven nanocomposite. The ternary photocatalyst's tetracycline degradation constant was 46.1-fold greater than TiO_2's. The photoluminescence and electrochemical analysis demonstrated increased segregation of charges and easy transfer, that is due to the formation of n-n-p ternary photocatalyst. Additionally, the combination of Bi_2O_3 and $MgBi_2O_6$ (less band gap) with TiO_2 (large band gap) resulted in the generation of more charge carriers. Compared to the pristine components, this ternary composite exhibited good degradation efficiency for other pollutants also, like Methyl orange, Methylene blue, and Rhodamine-B dye [34].

Ayappan *et al.,* 2020 employed a wet-impregnation method to prepare rod-shaped n-type α-Ag_2WO_4 with the combination of p-type Sb_2S_3 chalcogenide. They showed that compared to pure Ag_2WO_4, adding Sb_2S_3 improves the light harvesting ability of the synthesised composites. Among the nanocomposites, Sb_2S_3/α-Ag_2WO_4 (25 wt.%) exhibits the highest photocatalytic degradation efficiency, with ~ 91% degradation of MB dye with the irradiation time of 60 min. The rate constant for this photocatalyst is 5.7 and 3.7 times higher as compared to α-Ag_2WO_4 and Sb_2S_3, respectively. When unveiled to the colorless toxic contaminant Tetracycline hydrochloride, Sb_2S_3/α-Ag_2WO_4 photocatalyst achieved a degradation of 53.06% in 180 min, with approximately 4.1 x 10^{-3} min^{-1} rate constant. Radical trapping measurements revealed that the critical reactive moeties in this photocatalyst are h^+ and $^{\bullet}O_2^-$, which efficiently decompose the pollutant [30].

Xiao *et al.,* 2022 successfully created Sb_2S_3-$ZnIn_2S_4$ heterostructure using a one-step hydrothermal method. This structure consists of $ZnIn_2S_4$ nanosheets uniformly growing onto Sb_2S_3 nanorods, resulting in a closely bonded interface. The heterostructure enhances light absorption, increases surface area, reduces electron transmission distance, and promotes efficient migration and separation of photoexcited carriers. Notably, the optimal Sb_2S_3-$ZnIn_2S_4$ sample exhibits an impressive photocatalytic H_2 production rate of 1685.14 µmol/g/h. This photocatalyst showed remarkable removal efficiency, reaching 85.36% for Tetracycline hydrochloride. Moreover, it displayed excellent degradation capabilities for Oxytetracycline (80.52%) and 2-Mercaptobenzothiazole (84.30%) with the help of visible light for approximately 140 min. These findings highlight the significant potential of the nanocomposite catalyst for environmental remediation applications [35].

Xiangwei Li *et al.,* 2023 generated Bi_2S_3/Sb_2S_3 nanocomposite hydrothermally. The Bi_2S_3/Sb_2S_3 heterojunction demonstrated high degradation performance under visible light irradiation. They completely degraded MB (30 min), RhB (60 min), and MO (120 min) in water. Additionally, these heterojunctions could reduce a 20 ppm Cr^{6+} solution in just 80 min. Moreover, the heterojunctions exhibited an outstanding H_2O_2 production, surpassing individual Bi_2S_3 by 1.9 times and Sb_2S_3 by approximately 1.7 times. These astounding findings can be due to the thoughtful planning and assembly of 0D/1D Bi_2S_3/Sb_2S_3, which increases the segregation and transfer of charge carriers generated due to exposure to light, broadens the spectrum of light absorption, and offers a sufficient number of active sites for improved redox activities. [36].

Makhloufi *et al.,* 2022 prepared Sb_2S_3-$Sb_4O_5Cl_2$ photocatalyst through a hydrothermal method, and they evaluated its efficacy in removing crystal violet dye from the water. Their prepared samples underwent analysis through UV-Visible measurements, scanning electron microscopy, and X-ray diffraction. The results verified the successful formation of the desired binary composite system, displaying a distinct morphology. When exposed to visible light, the Sb_2S_3-$Sb_4O_5Cl_2$ composite particles effectively degraded crystal violet dye in aqueous solutions. The value of absorbance of the dye decreased significantly from 1.263 to 0.084, indicating successful photodegradation. The compostie was exposed to visible-light for 270 min. This was further supported by the removal of the characteristic color of the dye. The Sb_2S_3-$Sb_4O_5Cl_2$ composite achieved a high removal efficiency of 96.24% for crystal violet after 270 min [29].

Dashairya *et al.,* 2020 investigated the photocatalytic elimination of Rhodamine-B dye using binary samples of $Bi_xSb_{2-x}S_3$ where the value of x can be 0.536, 1.09, and 1.68. It was done under visible light. Analysis of the phases and microstructure confirmed the presence of solid-solution phases, namely $Bi_{0.536}Sb_{1.464}S_3$, $Bi_{1.09}Sb_{0.91}S_3$, and $Bi_{1.68}Sb_{0.32}S_3$, exhibiting nanorods having diameter of approx 25-50 nm. The synthesized products showed exceptional photocatalytic performance, achieving remarkable degradation of Rhodamine-B with degradation levels ranging from about 95% to 99.5% within a 30 min. timeframe. They confirmed the full elimination of pollutant through analysis of carbon dioxide generated after photodecomposition, as determined by gas chromatography analysis [37].

Upon comparing our work with the previously reported studies listed in **Table 2.1,** it becomes evident that our catalyst not only outperforms them but also demonstrates

exceptional efficacy even at lower dosages. The combination of Bi_2O_3 with Sb_2S_3 proves to be an outstanding choice, yielding superior results in our research.

Table 2.1 List of various Bi_2O_3 and Sb_2S_3-based photocatalysts reported in the literature.

Photocatalyst synthesized	Pollutant decomposed	Catalyst Conc. (g/L)	Source of light	Time (min)	Degradation efficacy(%)	Rate constant (min^{-1})	Ref.
PANI@Bi_2O_3-BiOCl	Methylene Blue	0.5	Solar	120	80	0.012	[38]
α-Bi_2O_3/C-dots	Indigo Carmine Dye	1	Visible	120	86	0.01734	[39]
Ag_2O/Bi_2O_3	Methyl Red	75	Solar	40	93.22	2.148	[40]
$BiVO_4/Sb_2S_3$	Tetracycline	0.3	Solar	120	88.7	0.01557	[19]
$Sb_2S_3/Sb_4O_5Cl_6$	Crystal violet dye	-	Visible	270	96.24	-	[29]
Sb_2S_3/rGO Sb_2S_3/PCS	Rhodamine-B	1	Solar	150	89,77.6	0.013, 0.0091	[13]

CHAPTER 3 - MATERIALS AND METHODOLOGY

3.1 Chemicals and materials

Sodium hydroxide (NaOH) and sodium sulfate (Na_2SO_4) were purchased from Merck. Bismuth nitrate pentahydrate ($Bi(NO_3)_3.5H_2O$) and thioacetamide (C_2H_5NS) were procured from Spectrochem, India. Antimony trichloride ($SbCl_3$), tartaric acid ($C_4H_6O_6$), and RhB dye were purchased from Loba Chemie. Commercial TC powder was taken from Sigma Aldrich. TC tablets (concentration 250 mg) manufactured by Abbott's company, with the active ingredient Restecline 250, were used. Ultrapure double-distilled water was utilized for preparing the solutions. High-purity reagents were employed unadulteratedly.

3.2 Synthesis of Bi_2O_3 powder

About 2 mmol of $Bi(NO_3)_3.5H_2O$ and 3 mmol of Na_2SO_4 were dispersed in 40 ml de-ionized water. The resulting solution was magnetically agitated for 45 min at room temperature. Subsequently, After that, 40 mL of DI water was used to dissolve 18 mmol of NaOH and it was introduced drop by drop to the above-prepared solution accompanied by continuous swirling. The resultant product was heated in a Teflon-lined stainless steel autoclave for 12 h at 120°C. Eventually, the obtained slurry was washed thrice with DI water and once with ethanol, followed by drying in a oven at 80°C [41]. Finally, a pale yellow powder was collected and was identified as BO.

3.3 Synthesis of Bi_2O_3/Sb_2S_3 hybrid powder

The Bi_2O_3/Sb_2S_3 (BOSBS) hybrid material was prepared hydrothermally. Firstly, a uniform solution was formed by dissolving 0.0016 mol of Bi_2O_3 in 80 mL of distilled water. Under vigorous agitation, 0.0016 mol of $SbCl_3$, 0.010 mol of $C_4H_6O_6$, and 0.0032 mol of CH_3CSNH_2 were introduced to the above prepared solution, followed by ultra-sonication for 1 h. The entire solution was then subjected to heating at 180°C for 8 h in an autoclave made of stainless steel lined with Teflon. Afterwards, the mixture was then dried at 60°C in an oven after being rinsed three to four times with DI water and then ethanol. The resultant black colored powder material

was tagged 11BOSBS. Calculations were made for the chemical amounts needed to create the various mole ratios like 1:3, 3:1, and 1:5, then they successfully synthesized and were tagged as 13BOSBS, 31BOSBS, and 15BOSBS, respectively.

Similarly, bare Sb_2S_3 was synthesized as a reference in an analogous way but without the addition of Bi_2O_3. This dark purple-colored Sb_2S_3 powder was labeled SBS.

3.4 Characterization methods

The X-ray diffraction (XRD) of materials was conducted utilizing the PAN analytical X′ Pert-Pro diffractometer. The XRD instrument utilized Cu Kα radiation at 45 kV, with a scan ranging from 10 to 90 degrees and 0.026 degrees step size. The wavelength used for the analysis was 1.5406 Å. For transmission electron microscopy (TEM) study, the Thermofisher (TALOS F200S G2) instrument was employed. It was operated at 200 KV, featured a field emission gun (FEG), and utilized a CMOS camera with a resolution of 4 K × 4 K. The analysis also involved a column energy-dispersive X-ray spectroscopy (EDS) detector. To demonstrate nitrogen sorption characteristics, the Microtrac Belsorp Mini-II surface area analyzer from Bel, Japan, was utilized. The materials underwent pre-treatment in a nitrogen environment at 100 degrees Celsius for 5 hours to ensure the absence of unwanted contaminants and gases. The distribution of pore size was examined using the Barrett-Joyner-Halenda (BJH) method, while the surface area was found through the Brunauer-Emmett-Teller (BET) method. The morphological studies of the catalyst were assessed using the JEOL instrument JSM-6510, operating at a voltage of 15 kV. Color mapping images were also generated using this instrument. The color spectra of the desirable sample were inspected using Scanning electron microscopy - Energy-dispersive spectroscopy (SEM-EDS). pH measurements were performed using the cyber scan pH 1100 meter from Eutech, Singapore. UV-Vis diffuse reflectance spectroscopy (DRS) was done using the Hitachi-3900H spectrophotometer in diffuse absorbance mode. The oxidation states of metal oxides were analyzed using the PHI5200 X-ray photoelectron spectroscopy (XPS) system, that employed an Omicron ESCA apparatus with a monochromatic Al K X-ray source (1486.7eV). PerkinElmer LS-55 PL spectrometer was used to carry out Photoluminescence (PL) spectroscopic studies with an excitation wavelength of 330 nm for the catalyst. The kinetics of the materials were examined using the Shimadzu UV 2600 spectrophotometer. This analysis focused on the photocatalytic elimination of organic toxicants using sunlight. Total organic

carbon (TOC) was measured using the Multi N/C 2100 BU TOC analyzer from Analytik Jena AG Corporation.

3.5 Photocatalytic deterioration of organic pollutants

For assessing the photocatalytic efficiency of BOSBS, decomposition of recalcitrant contaminants, RhB and TC was carried out using natural sunlight conditions. Initially, 3 mg of photocatalyst was dissolved into 10 mL of RhB solution (5 ppm) and 10 mL of TC solution (10 ppm) at the concenteration of 0.3 g/L. Prior to irradiation, both solutions were gently stirred in dark (60 min) to accomplish equilibrium in the adsorption-desorption phenomenas. The solution was then agitated for 120 min with the vessel horizontal in the sunlight to carry out the degradation process. Approximately 3-4 mL of the solution was extracted time to time and was analyzed using UV-visible spectrophotometer after the removing the BOSBS catalyst.

The photocatalysis experiment was conducted at Thapar University, Patiala, India, situated in a sub-temperate area. The study took place from March 15, 2023, to April 10, 2023. A LICOR pyranometer was used to measure the average solar radiation intensity and was found to be 850 W/m². The experiments were repeated three times, and graphs were plotted, incorporating error bars having a 5% data source error. The absorbance spectra of RhB and TC was taken at regular intervals, specifically at λmax = 554 nm and 360 nm, respectively. The assessment of degradation efficacy was done using the **Eq. (3.1).**

$$\% \, Deg = \{(Ab_0 - Ab_t)/Ab_0\} \times 100 = \{(C_0 - C_t)/C_0\} \times 100 \qquad \textbf{(3.1)}$$

Here, % Deg represents the degradation efficacy, Ab_0 denotes the initial absorbance, and Ab_t represents the absorbance at time 't'. Similarly, C_0 indicates the initial concentration, while C_t signifies the concentration at time 't'.

The effectiveness of the photocatalytic treatments for RhB and TC was evaluated by conducting Total Organic Carbon (TOC) and Chemical Oxygen Demand (COD) analysis. 60 mg of the 13BOSBS photocatalyst added to 200 mL solution was first exposed to sunlight for 120 min prior to the investigation. Ater the irradiation, the resulting sample was then subjected to the standard protocols of TOC and COD. The COD was determined using a titration technique,

while the degree of mineralization was assessed through TOC removal. The percentage of COD and TOC reduction was calculated using the **Eq. (3.2) and (3.3).**

$$\% \, COD = \{(COD_i - COD_f)/COD_i\} \times 100 \qquad \textbf{(3.2)}$$

$$\% \, TOC = \{(TOC_i - TOC_f)/TOC_i\} \times 100 \qquad \textbf{(3.3)}$$

Here, COD_i, COD_f, TOC_i, and TOC_f represents the initial and final values of COD and TOC, respectively.

CHAPTER 4 - RESULTS AND DISCUSSIONS

4.1 XRD analysis

The XRD pattern depicted in **Fig. 4.1** elegantly provided a clear verification of the purity and crystalline arrangement of the synthesized composites.

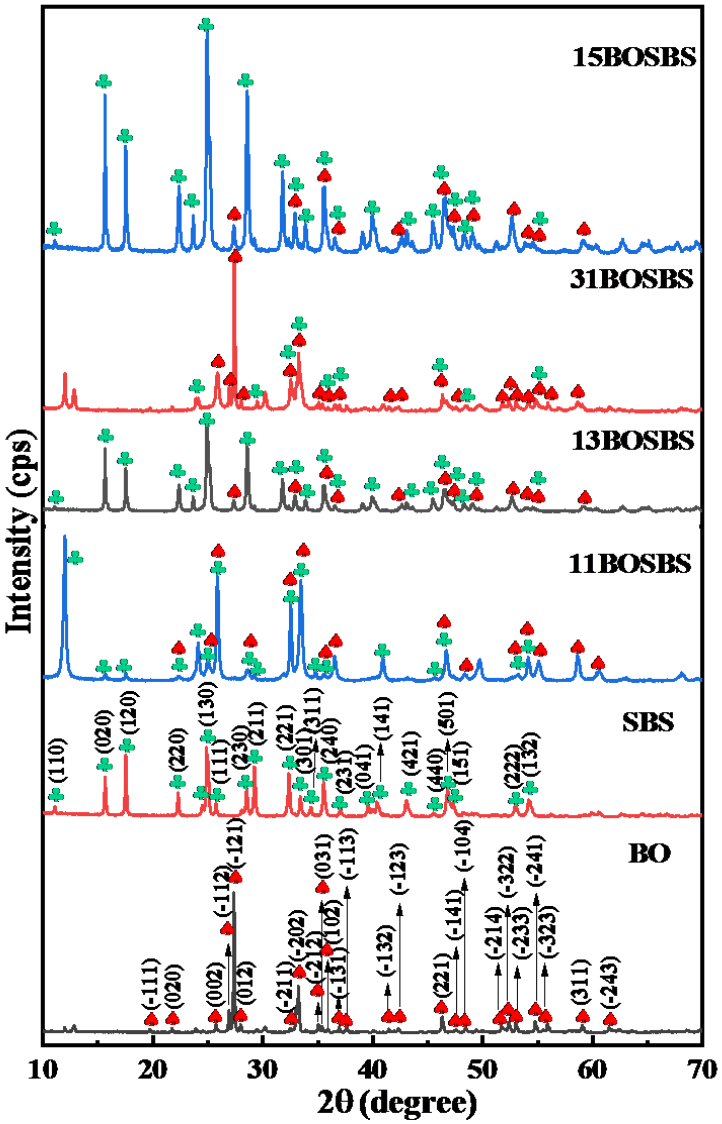

Fig. 4.1 XRD spectra of pure BO, SBS, 11BOSBS, 13BOSBS, 31BOSBS, and 15BOSBS composites.

The successful fabrication of monoclinic BO was approved by the existence of peaks at 19.7° (-111), 21.7° (020), 25.65° (002), 26.9° (-112), 27.4° (-121), 28.06° (012), 32.4° (-211), 33.2° (-202), 35.0° (-212), 35.3° (031), 35.9° (102), 36.8° (-131), 37.5° (-113), 46.2° (221), 51.7° (-214), 52.3° (-322), 53.1° (-233), 54.8° (-241), 56.0° (-323), 59.1° (311), and 61.6° (-243). correspond to the JCPDS card 01-071-0465. The diffraction peaks observed at the crystallographic planes, namely 11.04° (110), 15.62° (020), 17.58° (120), 22.27° (220), 24.4° (101), 24.88° (130), 25.77° (111), 28.4° (230), 29.26° (211), 32.42° (221), 33.3° (301), 34.3° (311), 35.5° (240), 36.9° (231), 39.5° (041), 40.3° (141), 43.1° (421), 45.4° (440), 46.8° (501), 47.3° (151), 52.9° (222) and 54.2° (132) are in agreement with the JCPDS card having number - 00-006-0474. This ensures the successful formation of SBS having orthorhombic structure. The persistence of sharp peaks indicated the crystalline nature of the photocatalysts. Also, both types of peaks were observed in the composites. No impurity peak as further detected indicating the successful fabrication of the composites. Moreover, minimal peak shifting was observed, suggesting the exceptional purity of the binary heterojunction photocatalysts and their two-phase composition.

4.2 XPS studies

The elemental make-up, the core electrons' binding energy, and the oxidation state of the elements were all investigated using XPS analysis. XPS can discern the spin-orbit splitting of metal ions in two distinct forms characterized by varying binding energies. **Fig. 4.2(a)** illustrates the survey spectrum of the as-synthesized composite. The discernible peaks indicate that the 13BOSBS composite primarily comprises bismuth, oxygen, antimony, and sulphur. The instrument's adventitious carbon is responsible for the C 1s signal at 284.7 eV. A least-square Gaussian-fit model was employed for deconvolution purposes. The presence of deconvoluted peaks in the spectra of bismuth (Bi) and oxygen (O) at the binding energies of 159.3 and 164.7 eV **(Fig. 4.2(b))** and 531.9 eV **(Fig. 4.2(c))** can be attributed to the Bi $4f_{7/2}$ and $4f_{5/2}$ [42,43] and O 1s [44], respectively. These findings show that Bi and O, respectively, are in the +3 and -2 oxidation states. These peaks verify the accomplished formation of BO within the composite. **Fig. 4.2(d)** illustrates a doublet peak observed at binding energies of 529.8 and 539.2 eV, which can be attributed to antimony (Sb) $3d_{5/2}$ and $3d_{3/2}$, respectively indicates the +3 oxidation state of Sb [45,46]. **Fig. 4.2(e)** depicts doublet peak of sulphur (S) spectrum, precisely positioned at 161.3 and 165.1 eV corresponds to the S $2p_{1/2}$ and $2p_{3/2}$ states, respectively, associated with the

−2 oxidation state [47,48]. This demonstrates that the SBS in the composite was successfully synthesized.

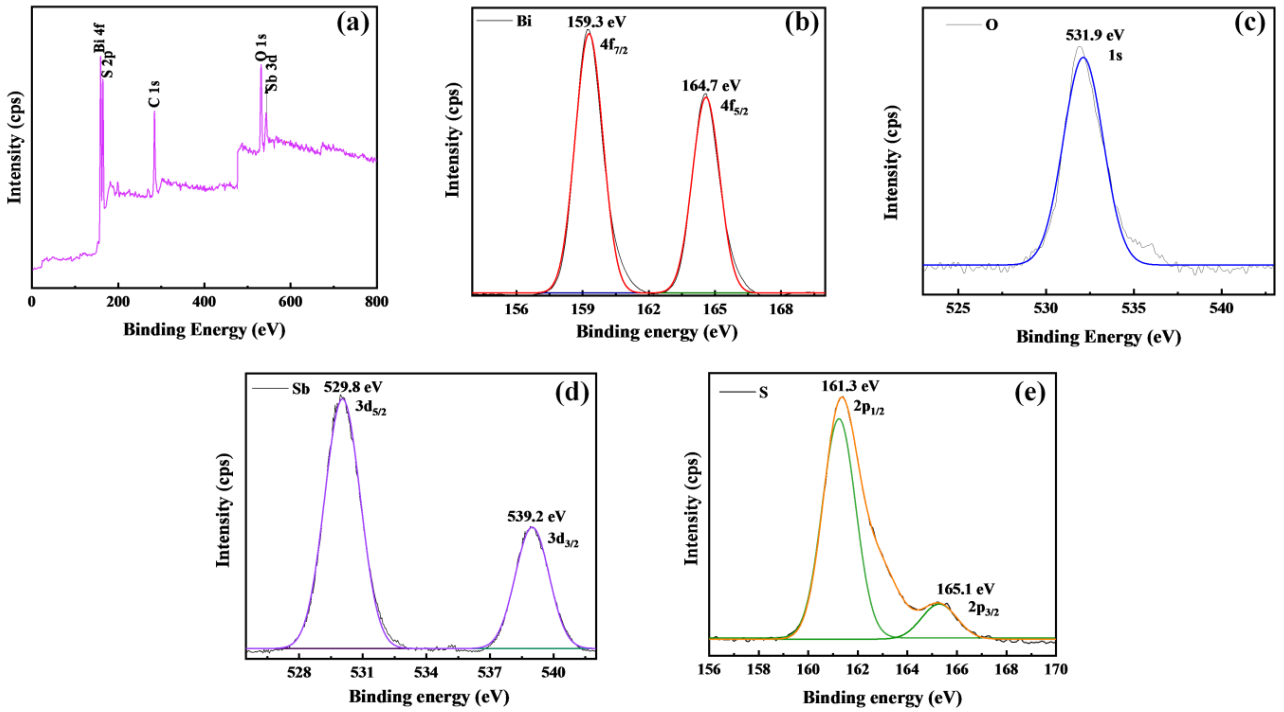

Fig. 4.2(a-e) XPS spectra of 13BOSBS, **(a)** survey spectra, **(b)** Bi 4f, **(c)** O 1s, **(d)** Sb 3d, and **(e)** S 2p.

4.3 Nitrogen sorption analysis

The surface area properties and distribution of the size of the pores of the produced samples were evaluated through nitrogen sorption experiments. The photocatalysts demonstrate a type-IV nitrogen adsorption curve, indicating their mesoporous nature as illustrated in **Fig. 4.3(a)** and **(b).** The determination of size of the pores was accomplished by employing the BJH plot. **Table 4.1** presents a summary of the specific surface area results, mean pore diameter, and pore volume. It was found that 13BOSBS and 15BOSBS hetero-composites exhibited similar and exceptionally high specific surface area out of all the bare materials and the other synthesized photocatalysts. Heterojunction photocatalysts' large surface area allows for improved interfacial contact between the two components, thereby, promoting efficient charge migration. Additionally, the ample number of exposed surface-active sites facilitates the adsorption of an immense amount of pollutant, resulting in improved photocatalytic performance [49].

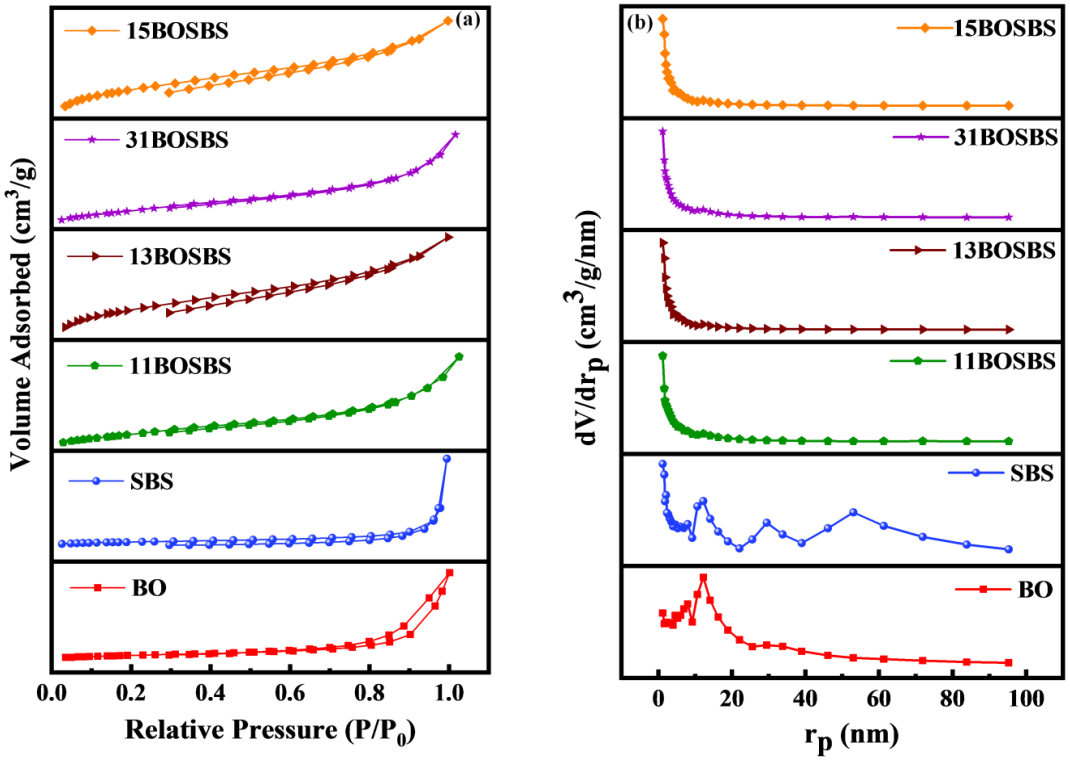

Fig. 4.3(a) BET surface area isotherm, and **(b)** BJH plot for pore size determination of the synthesized photocatalysts.

Table 4.1 Surface properties of the fabricated photocatalysts.

Sample	Pore Diameter (nm)	Specific Surface Area (m^2/g)	Mean Pore Volume (cm^3/g)
BO	14.44	30	0.478
SBS	11.85	18	0.321
11BOSBS	15.32	46	0.358
13BOSBS	23.40	57	0.434
31BOSBS	18.21	49	0.404
15BOSBS	24.01	59	0.458

4.4 SEM and TEM analysis

The SEM analysis examined the surface topography of BO, SBS, and 13BOSBS composite at varying magnifications. The results revealed that BO exhibited a morphology with larger nano-

rods **(Fig. 4.4(a))**, while SBS displayed smaller nano-rods like morphology **(Fig. 4.4(b)).** While, in the in-situ 13BOSBS composite, smaller nano-rods were observed to be loaded onto larger nano-rods as shown in **Fig. 4.4(c,d).** Both morphologies are present in the composite, which supports the successful creation of the heterojunction. Moreover, this dual morphology offers numerous active sites, thereby, increasing the pollutant adsorption and enhancing the photocatalytic degradation activity.

TEM analysis also confirmed the successful synthesis of the composite, showing smaller nano-rods of SBS decorated onto larger nano-rods of BO as depicted in **Fig. 4.4(e, f).**

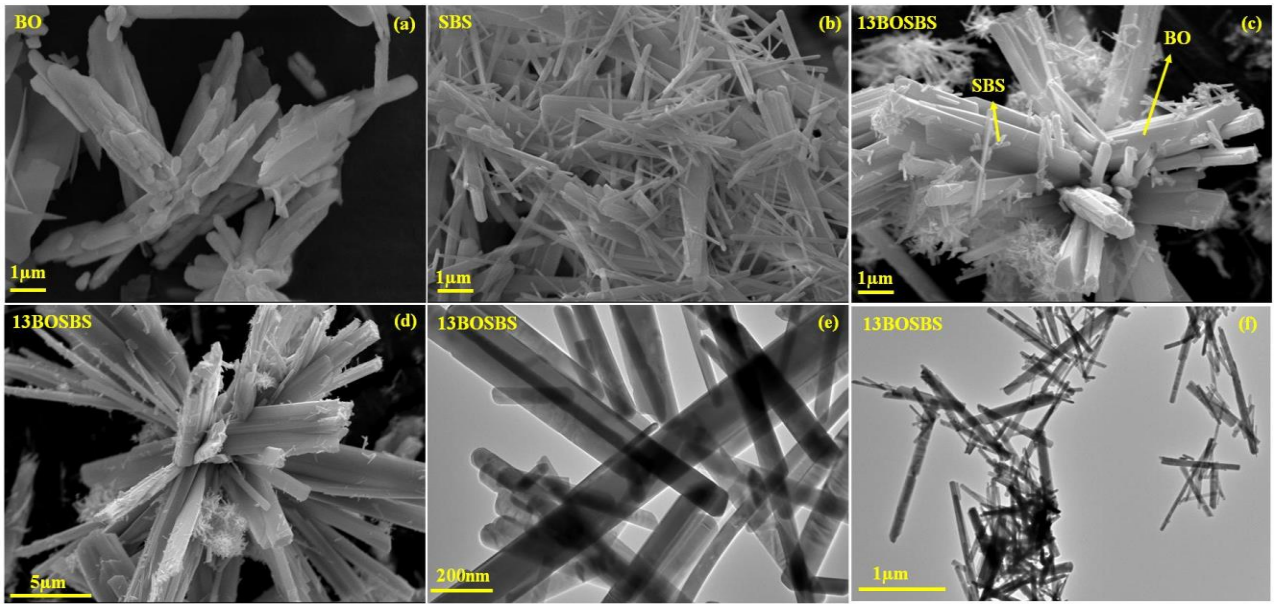

Fig. 4.4 SEM images of **(a)** BO, **(b)** SBS, **(c, d)** 13BOSBS composite, and **(e, f)** TEM images of 13BOSBS composite.

4.5 EDS and elemental mapping

The distribution of elements, composition, and the purity of the prepared photocatalyst were assessed using EDS. **Fig. 4.5(a)** shows that the EDS spectrum exhibited prominent signals of Bi, O, Sb, and S. The lack of any additional elemental peaks in the EDS spectrum demonstrates that the surface of the synthesised composite is free of impurities and serves as proof that the fabrication process was effective by showing that the surface is devoid of impurities. The SEM image of the composite closely fits the geographical distribution of Bi, O, Sb, and S, illustrating a uniform distribution of all the elements as depicted in **Fig. 4.5(b-e).** These findings represent

an excellent dispersion of SBS onto BO, which is highly advantageous for a heterojunction photocatalyst.

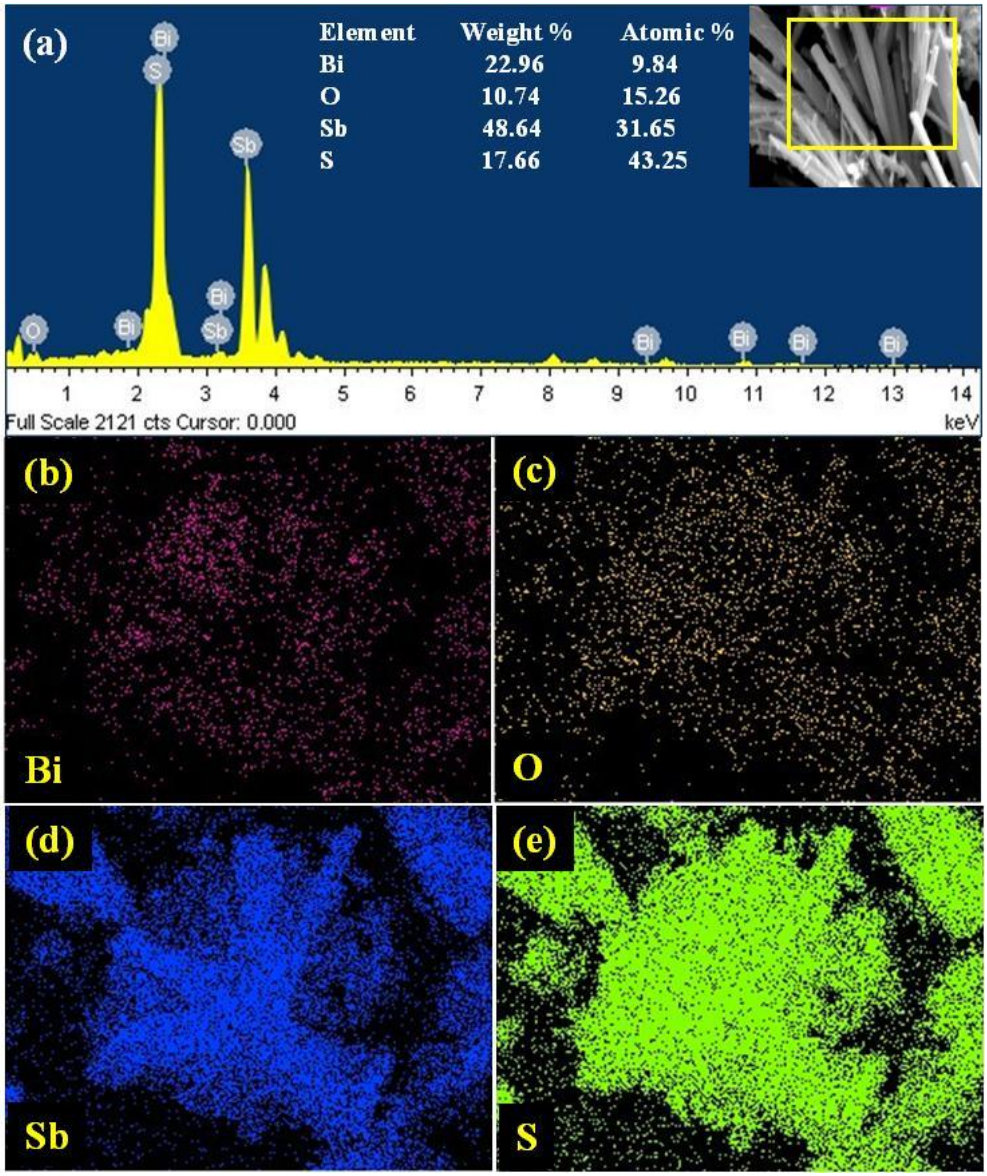

Fig. 4.5(a) EDS spectrum of the 13BOSBS heterojunction with the corresponding SEM image, and **(b–e)** mapping of elements of the 13BOSBS composite.

4.6 PL analysis

The PL spectra was done to find out the migration, separation, and recombination of charge carriers [50]. A good photocatalyst should possess a lower rate of reassimilation, a high capacity for transporting charge carriers, and effective charge segregation [51]. The PL signal's emission intensity is a direct reflection of the exciton recombination rate. A low emission intensity

indicates a reduced rate of recombination of the electrons and holes, leading to enhanced charge transfer efficiency and improved photocatalytic performance [52]. In this study, the PL spectra were taken using an excitation wavelength of 330 nm. **Fig. 4.6** shows that pure BO and SBS displayed the maximum PL intensity. The 13BOSBS and 15BOSBS photocatalysts exhibited similar yet the lowest PL intensities among all the samples suggesting their lower recombination rate, efficient charge segregation, and superior charge carrying ability. This is due to the formation of a heterojunction between BO and SBS. Furthermore, on adding more of SBS in the composite, PL intensity got reduced significantly, illustrating that most photogenerated charge carriers were primarily sourced from SBS.

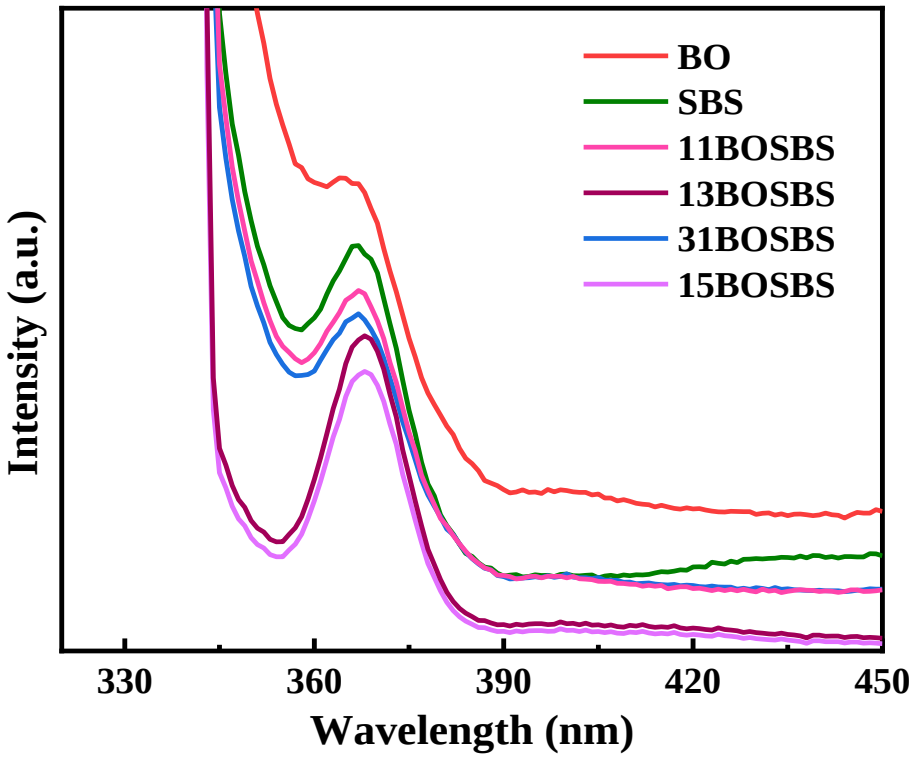

Fig. 4.6 PL Spectra of bare BO, SBS and fabricated BOSBS photocatalysts.

4.7 DRS studies

An efficacious photocatalyst must exhibit excellent light absorption strength and a narrow energy gap. DRS was done to scrutinize the absorption range and band gap. From the **Fig. 4.7 (a)**, it is evident that the synthesized photocatalysts exhibit notable visible light absorption capability. On enhancing the weight ratio of the SBS in the composite, a noticeable red shift was observed,

indicating their ability to absorb sunlight actively. The band gap energy was determined using Tauc's plot, which was obtained through the following **Eq. (4.1).**

$$(\alpha h\nu)^{1/2} = h\nu - E_g \qquad \textbf{(4.1)}$$

Here, α, h, ν, and E_g represent the absorption coefficient, Planck's constant, light frequency, and band gap energy, respectively. By extrapolating the Tauc plot to the photon energy (hν) axis, Eg values were determined. As a result, the band gaps of BO, SBS, 11BOSBS, 13BOSBS, 31BOSBS, and 15BOSBS were calculated as 2.62, 1.84, 1.70, 1.35, 1.62, and 1.29 eV, respectively, as illustrated in **Fig. 4.7(b).**

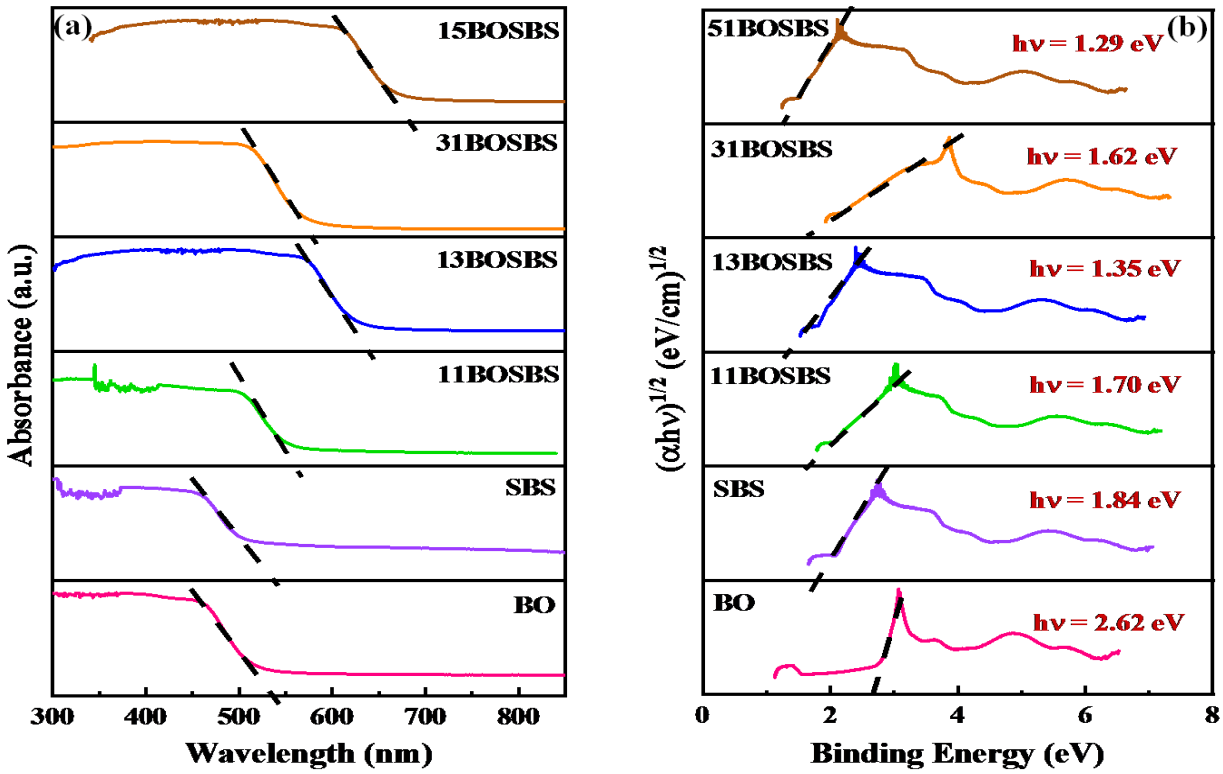

Fig. 4.7(a) UV-Visible DRS absorption spectra, and **(b)** the band gap energies of BO, SBS, 11BOSBS, 13BOSBS, 31BOSBS, 15BOSBS.

These findings indicate that 13BOSBS and 15BOSBS composites possess lesser band gap and highest visible light absorption capability among the synthesized photocatalysts. These two traits make these catalysts apt for photocatalytic degradation. Narrow band gap and high visible light absorption enhances their ability to carry out the photocataytic reactions smoothly.

4.8 Photocatalytic studies

4.8.1 Photocatalytic degradation of the model colored pollutant, RhB

Photocatalytic abatement of the model pollutant, RhB was done to scrutinize the performance of the photocatalysts. Initially, for the photolysis experiment, a solution containing 10 mL of 5 ppm RhB was exposed to sunlight for 120 min and only 25.9 % of RhB degradation was observed. While, in the existence of 13BOSBS, and 15BOSBS photocatalysts, highest degradation rate of 98.2% and 99 % was observed, respectively. The rate constant (k) was determined using the **Eq. (4.2).**

$$ln(C/C_0) = - kt \qquad \textbf{(4.2)}$$

where C_0 represents the initial concentration at time t = 0, C represents the concentration at a given time (t), and k is the rate constant.

Fig. 4.8(a) and **4.8(b)** depicts the kinetic analysis for the photocatalytic reduction of RhB. Hence, from **Fig. 4.8(b)**, it can be gauged that the reaction is following pseudo-first order kinetics. The 13BOSBS and 15BOSBS possessed the maximum rate constants of 0.03149 and 0.03876 min^{-1}, respectively out of all the fabricated photocatalysts. While both 13BOSBS and 15BOSBS displayed similar activity, the latter required a larger quantity of SBS, which has a more expensive precursor salt than the precursor salts required for the fabrication of BO. Therefore, further detailed photocatalytic experiments were conducted using 13BOSBS due to its cost-effectiveness compared to 15BOSBS. In contrast, a degradation experiment utilizing TiO_2-P25 was conducted In comparison, a degradation experiment employing TiO_2-P25 was carried out under comparable circumstances to evaluate the effectiveness of the generated composites in terms of degradation. The degradation efficiency achieved was 52%, with a corresponding rate constant of 0.00485 min^{-1}. To assess the level of synergistic effect in the composites, the synergy factor (R) was calculated using **Eq. (4.3).**

$$R = \frac{k_{BO}/k_{SBS}}{k_{BO} + k_{SBS}} \qquad \textbf{(4.3)}$$

Here, k, k_{BO}/k_{SBS}, k_{BO}, and k_{SBS} stand for the rate constant, the rate constant of hybrid BO and SBS, the bare BO, and SBS, respectively.

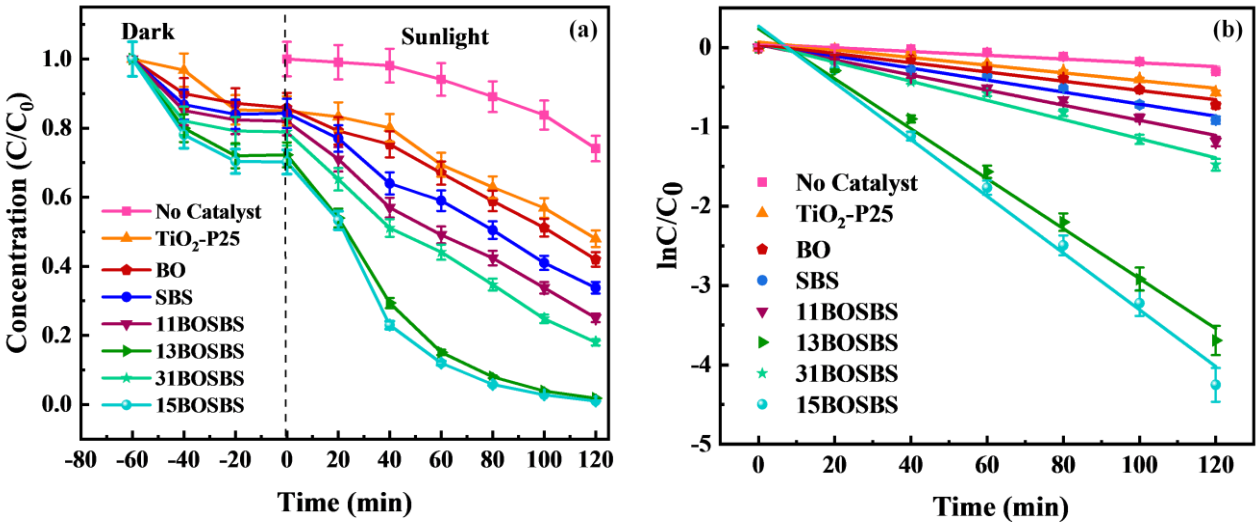

Fig. 4.8(a,b) Kinetic analysis of the synthesized photocatalysts for the degradation of RhB.

Table 4.2 The % degradation, rate and synergistic constants achieved by the photocatalytic removal of RhB.

Catalyst	Rate Constant (min^{-1})	Decomposition Efficacy (%)	R
TiO_2-P25	0.00485	52	-
BO	0.00583	58	-
SBS	0.00757	66.2	-
11BOSBS	0.00952	74.9	0.71
13BOSBS	0.03149	98.2	2.35
31BOSBS	0.01206	82	0.90
15BOSBS	0.03876	99	2.89
No Catalyst	0.00238	25.9	-

Among the prepared materials, 13BOSBS exhibited the highest R factor (2.35), indicating superior efficiency attributed to its strong synergistic effect on BO and SBS. This result indicates

that 13BOSBS outperformed TiO_2-P25 as the most efficient photocatalyst for degrading RhB. The degradation efficacy, rate constants, and synergistic constant values of the different photocatalysts are summarized in **Table 4.2.**

4.8.2 Impact of light sources

Under optimal conditions, comparative photocatalytic experiments were carried out with the help of different sources of light, including UV, visible, and natural sunlight. From the **Fig. 4.9,** it can be scrutinized that the pollutant decomposition reached to 69% under UV light and 83% under visible light. While, the maximum elimination of 98.2% was achieved under natural sunshine using the 13BOSBS heterojunction photocatalyst. These findings demonstrate that natural sunlight can effectively degrade the pollutant using the developed photocatalyst. Thus, the natural sunlight is remarkably significant over other artificial light sources in pollutant deterioration.

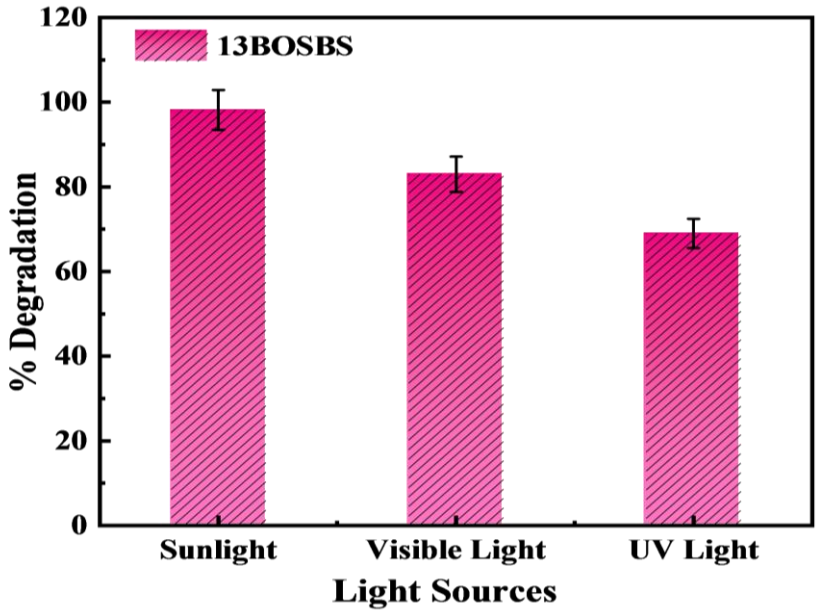

Fig. 4.9 The impact of diferent sources of light on the decomposition efficacy of RhB using the 13BOSBS photocatalyst.

4.8.3 Impact of concentration of the catalyst

The productiveness of the photocatalytic process is greatly linked to the precise quantity of catalyst employed. It is essential to use the optimal amount of catalyst to prevent its excessive

usage, which can lead to particle aggregation [19,53]. Additionally, employing the right amount ensures maximum photon absorption, promoting the efficient photodecomposition. Tests were done to see what effect the catalyst concentration, which ranged from 0.1 g/L to 0.6 g/L, had on the dye's photocatalytic degradation. From the **Fig. 4.10,** it can be observed that as the photocatalyst dose is enhanced from 0.1 g/L to 0.3 g/L, the degradation efficiency increases notably, reaching approximately 98.2% at 0.3 g/L. This is because of the augmentation in the number of reaction sites resulting from the increased catalyst amount. But as the concentration was raised to 0.4 g/L, the efficacy of the degradation decreased. It can be attributed to the solution becoming more opaque, which causes light to disperse and diminishing its influence on the solution. Also, the catalyst surface becomes saturated with dye through complete adsorption, therefore, additional incorporation of catalyst does not contribute to further degradation. It is because the active sites become deactivated and lose their effectiveness [54]. As a result, best concentration for future experiments was found to be 0.3 g/L of the photocatalyst.

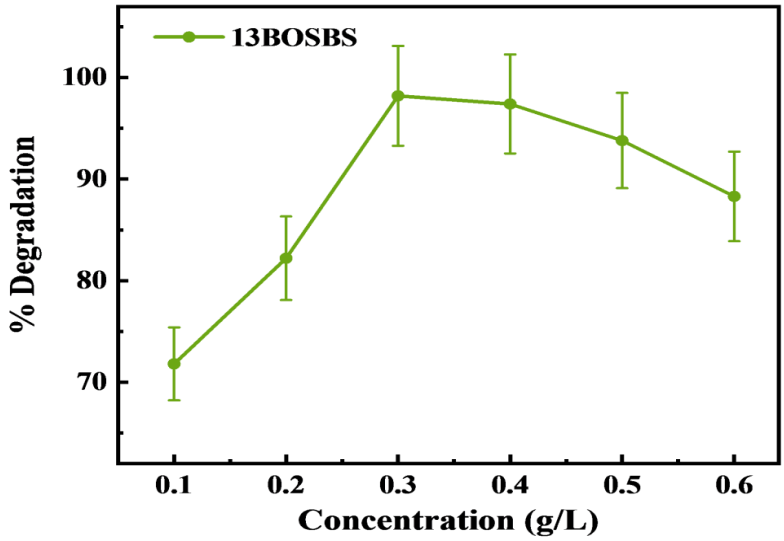

Fig. 4.10 Concentration impact of the 13BOSBS photocatalyst.

4.8.4 pH studies

The pH of the solution plays a crucial role in determining the photocatalytic performance of the catalyst. pH variations can modify the surface characteristics of the catalyst, affecting the adsorption of target compounds and potentially altering the degradation pathway [55]. Over a variety of pH values, including 2, 3, 4, 5, 6, 7 (natural pH), 8, 9, 10, and 11, the effect of pH on

the photocatalytic degradation of RhB as shown in **Fig. 4.11(b)** was investigated. The surface charge of the catalyst under various pH settings and the electrical charges of the pollutant can both be blamed for the observed pH fluctuations. The pH at which the surface of Bi_2O_3/Sb_2S_3 has a zero charge (pH_{pzc}) was determined to be 5.37, shown in **Fig. 4.11(a).** At pH values higher than 5.37, the dominant species on the oxide surface is M - O^-, where M represents the metal which favors the adsorption of cationic species due to electrostatic interaction. Conversely, at pH values lower than 5.37, the primary species were M - OH^{2+}, promoting the adsorption of anionic species [56]. The highest degradation efficiency of 98.2% was obtained for RhB at natural pH.

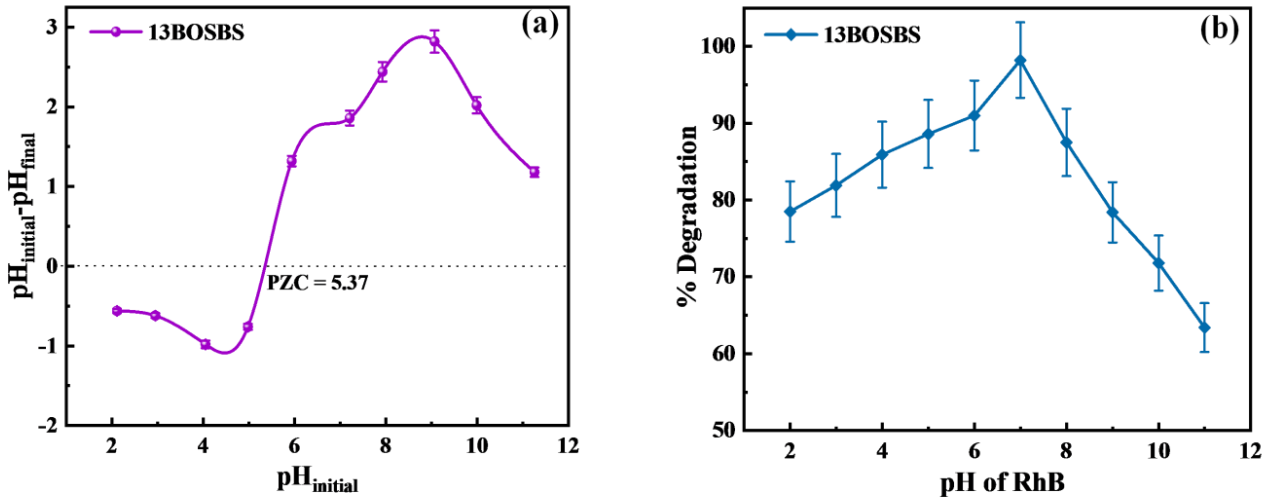

Fig. 4.11(a) pzc of the 13BOSBS nanocomposite, and **(b)** pH impact on the decomposition efficiency of the 13BOSBS photocatalyst.

RhB primarily exists as a cation (RhB^+) at pH below 3.7 (pka_{RhB}). However, it exists in zwitterionic form ($RhB^{\pm}$) at pH values above 3.7, which can be attributed to the deprotonation of the carboxyl group [57]. Within the pH range of 2 and 3, the cationic form of RhB repels the cationic surface of the catalyst, resulting in comparatively diminished degradation efficiency. Within the pH range of 3.7 to 5.37, the degradation efficiency increases as the anionic portion of the dye from the zwitterionic form gets adsorbed onto the cationic surface of the catalyst. Once the pH surpasses 5.37, the catalyst's surface acquires a negative charge. Now, the degradation efficiency is enhanced as the cationic component of the dye in its zwitterionic form becomes adsorbed onto the anionic surface of the catalyst. Thereby, the highest efficiency was attained at pH 7, but the degradation efficacy decreased beyond this pH. This decline can be attributed to

the repulsion between the anionic portion of the dye in its zwitterionic form and the anionic surface of the catalyst [57,58].

4.8.5 Scavenger studies

A scavenger experiment was conducted utilizing commonly employed quenchers to find out the function of the reactive radical moeties accountable for the photocatalytic elimination of the dye. In the photocatalytic reactions, chemical quenchers such as benzoquinone (BQ), methanol, and dimethyl sulfoxide (DMSO) were utilized at a concentration of 1 mM each to examine the function of superoxide radicals ($O_2^{-\bullet}$), holes (h^+), and hydroxyl radicals ($^\bullet OH$), respectively [59]. When no trapping agent was present, the dye exhibited a maximum degradation of 98.2%. However, the introduction of the aforementioned scavengers to the reaction medium effectively suppressed the rate of photocatalytic decomposition.

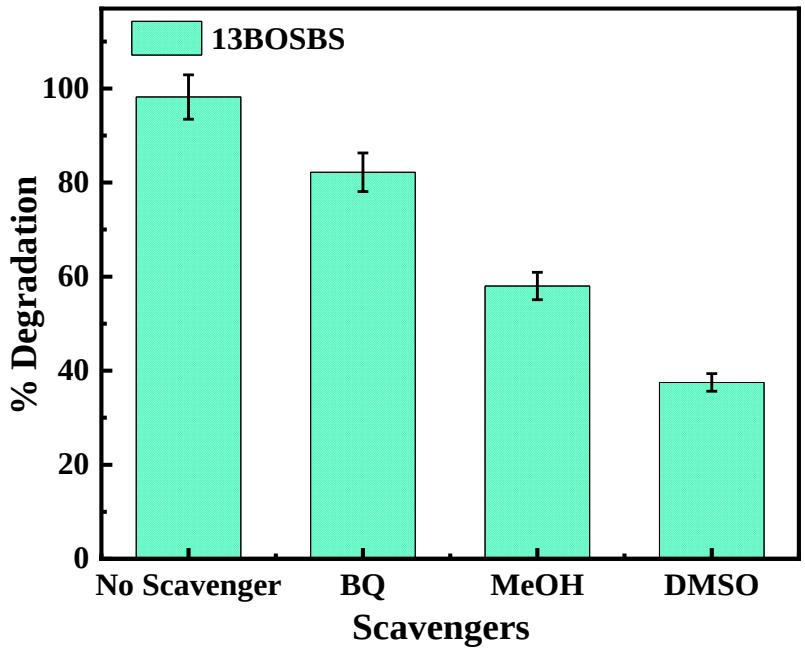

Fig. 4.12 Effect of different scavengers on the decomposition of RhB.

According to **Fig. 4.12,** the introduction of DMSO largely impacted the photocatalytic efficiency of the 13BOSBS composite, resulting in a reduction to 37.5% of the RhB. This finding suggests that $^\bullet OH$ radicals were the principal species accountable for the breaking down of the pollutant. Similarly, the presence of methanol also affected the degradation process, but to a lesser extent (58%), indicating that h^+ plays a minor yet significant role in eliminating the dye.

4.8.6 Reusability studies

Ensuring the longevity of a photocatalyst is crucial for its widespread practical implementation. Therefore, it is crucial to assess the catalyst's photocatalytic stability over a number of experimental deterioration cycles.

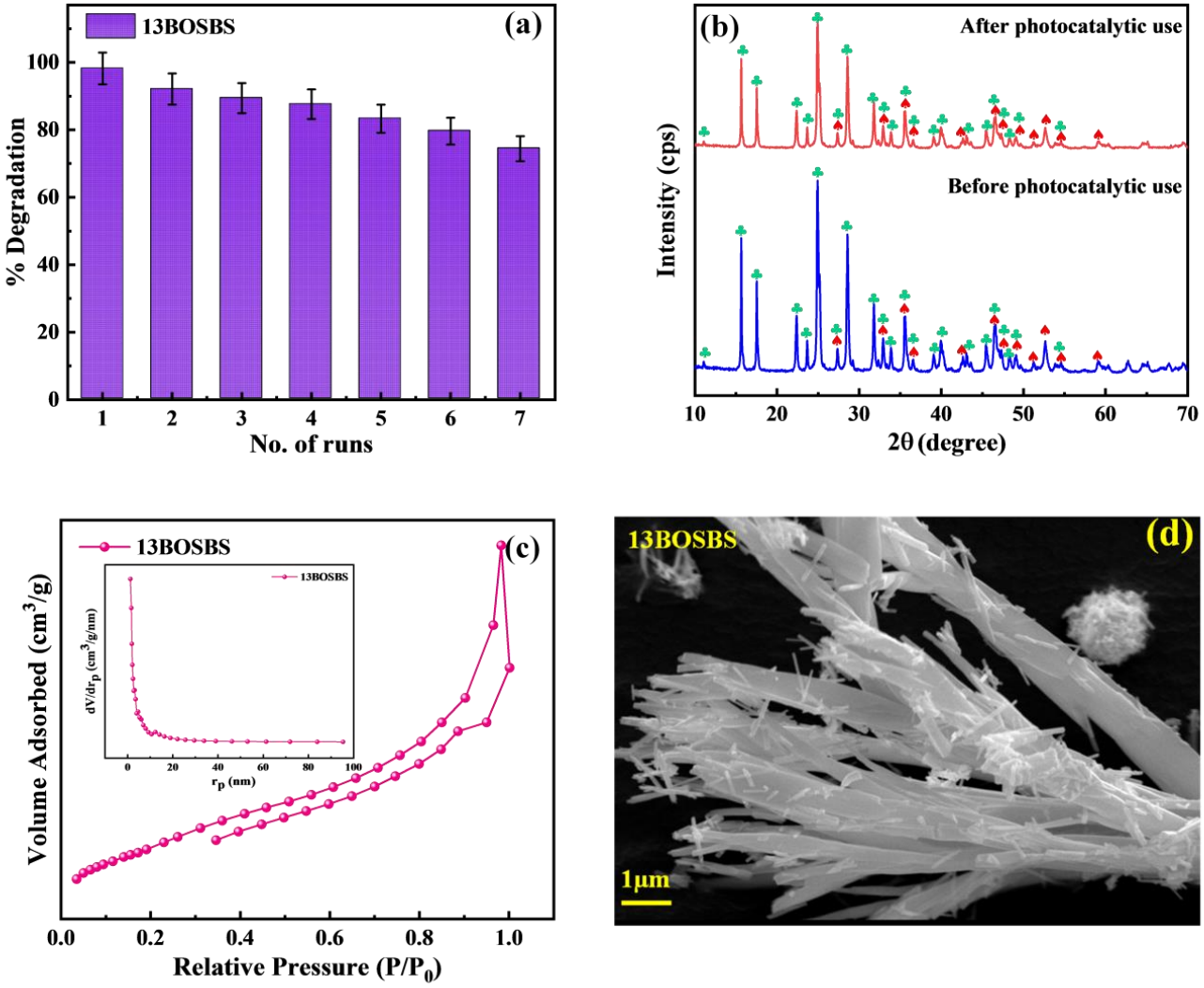

Fig. 4.13(a) Reusability graph, **(b)** XRD spectra of 13BOSBS composite after photocatalytic usage, **(c)** BET with inset showing BJH graph of 13BOSBS after deterioration activity, and **(d)** SEM image of the used catalyst after degradation studies.

Fig. 4.13(a) presents the findings of the reusability studies conducted on the 13BOSBS photocatalyst. The photocatalytic activity was evaluated under sunlight over seven degradation cycles lasting 120 min each. Due to physisorption of RhB onto the catalyst's surface, it can

easily desorbed from it. For renewal, the catalyst was thoroughly washed with DI water 3-4 times and subsequently dried at 60°C. This was done to vacate the catalyst's surface active sites for the next deterioration round. The initial decomposition of the pollutant was recorded at 98.2%. Remarkably, even after seven consecutive cycles, the catalyst maintained an impressive photodegradation efficiency of 74.4%. This observation highlights the catalyst's excellent reusability and stability. XRD analysis was done after the reusability studies revealed that peak positions and peak intensities remained the same, demonstrating that composite retained its nature even after the degradation studies **(Fig. 4.13(b)).** BET analysis revealed that the average pore volume was 0.343 cm^3/g. The surface area was found to be $51m^2/g$, and the pore diameter was 18.15 nm, for the 13BOSBS photocatalyst after the degradation studies. The BET studies are shown in **(Fig. 4.13(c)).** Although surface area got decreased, however, it was sufficient to carry out degradation. Furthermore, the SEM analysis confirmed that the morphology of the composite remained unchanged after the photocatalytic degradation experiments **(Fig. 4.13(d)).** Thus, the 13BOSBS photocatalyst exhibited reliable and stable photocatalytic performance.

4.8.7 Photocatalytic degradation of colorless pollutant (TC)

A photocatalytic degradation of the pharmaceutical pollutant, TC, was done to check the efficacy of 13BOSBS for the degradation of colorless contaminants in addition to dyes. Initially, a TC solution having 0.3 g/L of 13BOSBS photocatalyst was agitated in the dark (60 min) to accomplish the equilibrium in adsorption-desorption processes. The reaction was then carried out by exposing the solution to sunshine for 120 min. From **Fig. 4.14(a)** and **(b),** it was assessed that the maximum degradation efficiency of 91.5% was achieved with the rate constant of 0.01749 min^{-1}. These findings demonstrate that the as-prepared catalyst can effectively eliminate colorless contaminants, extending its applicability beyond dyes. This extends the applicability of the catalyst beyond just targeting dyes. The ability of the catalyst to effectively degrade colorless contaminants broadens its potential applications in water treatment and environmental remediation, where the presence of colorless pollutants is common. Overall, these results indicate that the 13BOSBS photocatalyst has promising properties for efficient contaminant degradation and highlights its potential for addressing a wider range of pollutants beyond colored compounds.

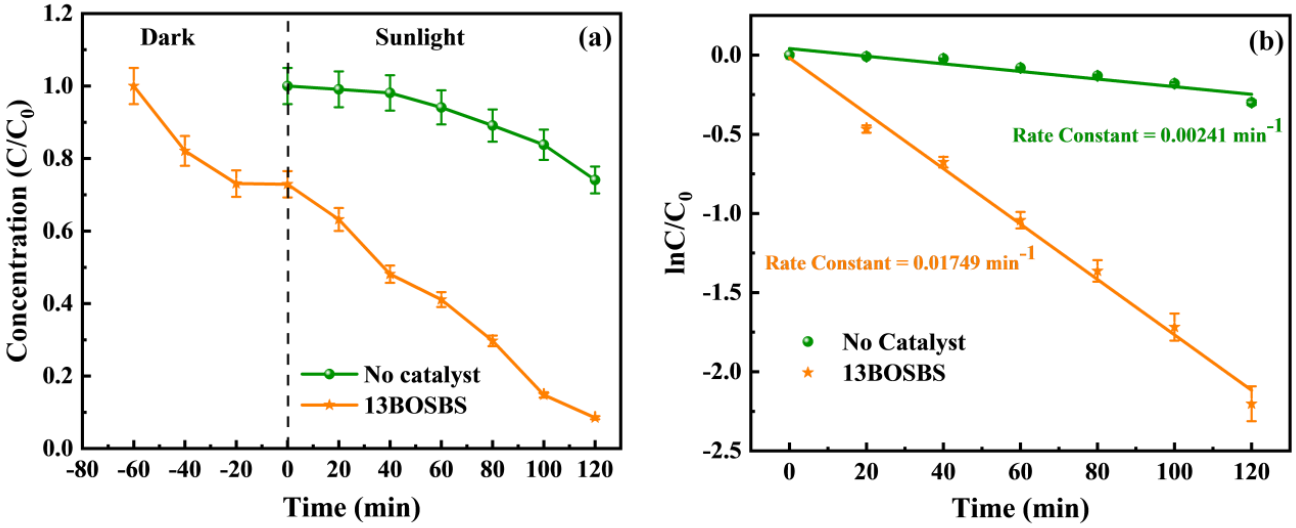

Fig. 4.14(a,b) Kinetic analysis of the 13BOSBS composite for the photocatalytic degradation of TC.

4.8.8 Mineralization studies

TOC was carried out to determine the extent of mineralization of RhB and TC by 13BOSBS composite. In the beginning, elevated levels of TOC and COD provided evidence that the contaminants RhB and TC contained a significant quantity of organic matter. For the RhB dye, the 13BOSBS photocatalyst reduced COD and TOC by 90.2 and 85%, respectively, when illuminated under solar light for 120 min. Similarly, the commercially available TC powder exhibited significant reduction of 84% in COD and 80% in TOC **(Fig. 4.15).** The creation of successive organic intermediates during the process, prior to the complete conversion of the target compounds (RhB and TC) into carbon dioxide and other simpler byproducts, caused the percentage of TOC eliminated to be lower than that of degradation [19]. Owing to limitations imposed by ethical permissions, actual experimentation using natural medical/pharmaceutical wastewater was not feasible. As an alternative, the effectiveness of the 13BOSBS photocatalyst in degrading a TC tablet (specifically, Abbott's Tetracycline capsules, I.P. Restecline 250, with 250 mg concentration) was evaluated through COD and TOC analysis, resulting in removal efficiencies of 78, and 73%, respectively. These findings validate the superior surface catalytic properties of the photocatalyst compared to the costly and time-harvesting physicochemical methods employed in the industry.

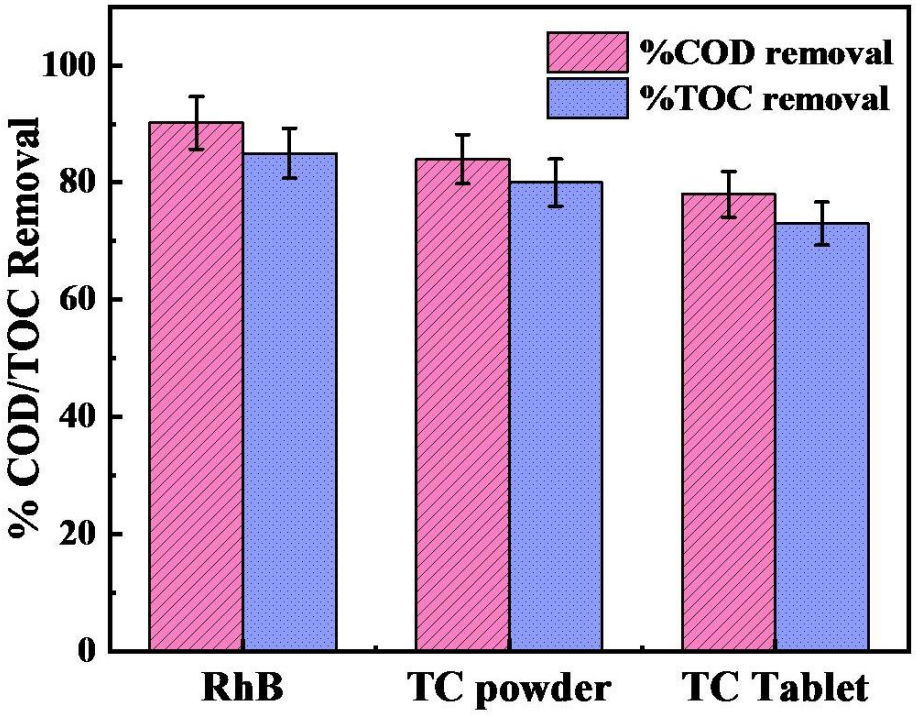

Fig. 4.15 COD and TOC analysis for RhB and TC.

4.9 Possible photocatalytic mechanism

The conduction band and valence band positions were determined by incorporating Mulliken's electronegativity value to gain insight into the charge transfer mechanism taking place in the BOSBS composite as indicated in **Eq (4.4) and (4.5).**

$$E_{VB} = \chi - E_e + 1/2E_g \quad \textbf{(4.4)}$$

$$E_{CB} = E_{VB} - E_g \quad \textbf{(4.5)}$$

Here, χ, E_{VB}, and E_{CB} represents Mulliken electronegativity, the valence band, and the conduction band's energy, respectively. E_e and E_g stand for the respective free electron energy on the hydrogen scale (4.5 eV) and band gap energy. The computed E_{CB} values for BO and SBS were 0.31 eV and 0.21 eV, respectively, while the E_{VB} values for BO and SBS were 2.93 eV and 2.05 eV, respectively. [60,61]. During exposure to light, the electrons present in the valence band of the semiconductors got transferred to their respective conduction bands. When both the semiconductors are near together, holes diffuse from the more positively charged valence band

of BO to the less positively charged valence band of SBS to prevent the reintegration of photogenerated charge carriers. Furthermore, electrons from more negatively charged conduction band of SBS migrate to the less negatively charged conduction band of BO. Consequently, these electrons in the conduction band of BO facilitate the reduction of oxygen, forming $O_2^{\bullet-}$ which can further react with water molecules, generating $^{\bullet}OH$ radicals. These oxidative species efficiently decompose RhB and TC, transforming them into H_2O, CO_2, and other degraded products that are less toxic. Further, the h^+ existing in the valence band of SBS react with water to generate $OH^{\bullet}$ which can oxidize harmful pollutant to simpler products. This possible mechanism is depicted in **Scheme 4.1.** As a result, the quick separation of electron-hole pairs and less recombination rate considerably improve the photocatalytic performance of BOSBS.

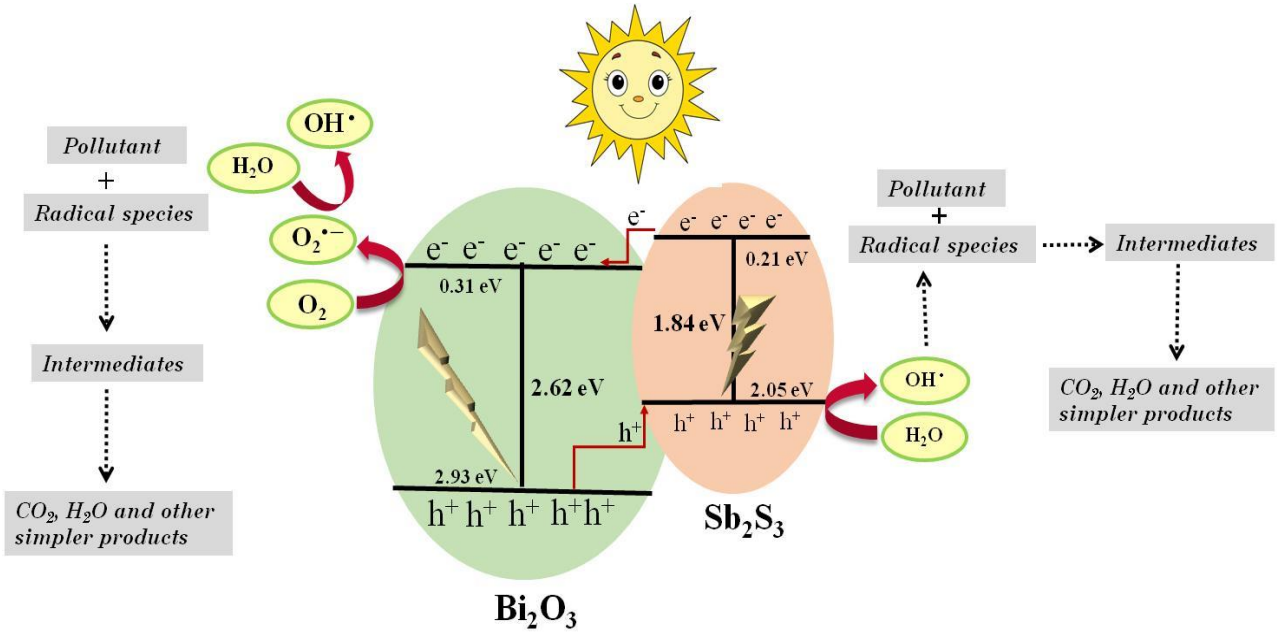

Scheme 4.1 Proposed route for the photodecomposition of contaminants by BOSBS composite.

CHAPTER 5 - CONCLUSIONS AND FUTURE SCOPE

The eco-friendly hydrothermal route was utilized to fabricate novel heterojunction Bi_2O_3/Sb_2S_3 photocatalysts with varying mole ratios. To validate the successful synthesis of the samples, a number of analytical methods, including XPS, DRS, SEM, EDS, TEM, XRD, and BET analysis were employed. SEM studies revealed that smaller nano-rods of SBS effectively loaded onto larger nano-rods of BO, were observed in the 13BOSBS composite efficiently forming a heterojunction. To assess the efficacy of the synthesized samples the photocatalytic decomposition of RhB and TC was conducted under the illumination of the natural sunlight. The concentration of SBS was found to have the direct impact on the decomposition efficacy, showing that as the concentration of SBS got increased, the decomposition effectiveness got improved. Among the fabricated photocatalysts 13BOSBS, and 15BOSBS demonstrated the highest photocatalytic decomposition efficacy with the highest rate constant value. However, due to the cost-effectiveness, 13BOSBS was considered the more efficient photocatalyst. According to PL, BET, and UV-visible DRS investigations, the composite effectively broke down contaminants when exposed to natural sunshine, which was attributed to its lesser recombination rate, high surface area, and adequate band gap. To further assess the superiority of the prepared nanocomposites, their decomposition efficacy was compared to that of the commercial TiO_2-P25. A range of experiments were conducted to investigate various factors affecting the photocatalytic degradation process. These include impact of catalyst concentration, effect of pH, kinetic studies, evaluation of different light sources, scavenger analysis, and assessment of the reusability of the catalyst. Trapping studies confirmed that $^{\bullet}OH$ were the main contributors effecting the degradation of the pollutant. The composite showed remarkable reduction efficacy even after seven trial cycles, emphasising its reusability for the photocatalytic eradication of organic pollutants. The composite maintained its original characteristics following the degradation studies, which was validated by XRD and SEM analysis, demonstrating physical adsorption of the dye onto the composite. Higher % COD and TOC removal demonstrate the catalyst's efficiency and superiority over industrial physicochemical methods. GC-MS analysis was conducted to study the products and intermediates resulting from the photodegradation experiments. Concisely, the BOSBS catalyst demonstrated efficient degradation of organic

pollutants using minimal quantities under the natural sunlight. Hence, it holds great potential for treating the challenging pollutants and industrial wastewater on a large scale. This catalyst has tremendous potential for a variety of wastewater treatment applications because it is affordable, simple to use, and environmentally benign. It offers a promising solution to prevent the persistent buildup of harmful toxic pollutants in water systems.

CHAPTER 6 - REFERENCES

[1] Sharma S, Basu S, Shetti NP, Kamali M, Walvekar P, Aminabhavi TM. Waste-to-energy nexus: A sustainable development. Environ Pollut 2020;267:115501. https://doi.org/10.1016/j.envpol.2020.115501.

[2] Akhundi A, Habibi-Yangjeh A, Abitorabi M, Rahim Pouran S. Review on photocatalytic conversion of carbon dioxide to value-added compounds and renewable fuels by graphitic carbon nitride-based photocatalysts. Catal Rev 2019;61:595–628. https://doi.org/10.1080/01614940.2019.1654224.

[3] Sharma S, Kundu A, Basu S, Shetti NP, Aminabhavi TM. Sustainable environmental management and related biofuel technologies. J Environ Manage 2020;273:111096. https://doi.org/10.1016/j.jenvman.2020.111096.

[4] Rathi A, Basu S, Barman S. Structural framework effect of various CeO_2-loaded zeolites on the adsorptive removal of fipronil. J Environ Chem Eng 2021;9:105167. https://doi.org/10.1016/j.jece.2021.105167.

[5] Wang Q, Li N, Tan M, Deng M, Yang G, Li Q, et al. Novel dual Z-scheme Bi/BiOI-Bi_2O_3-C_3N_4 heterojunctions with synergistic boosted photocatalytic degradation of phenol. Sep Purif Technol 2023;307:122733. https://doi.org/10.1016/j.seppur.2022.122733.

[6] Gao Z-Z, Qi N, Chen W-J, Zhao H. Construction of hydroxyethyl cellulose/silica/graphitic carbon nitride solid foam for adsorption and photocatalytic degradation of dyes. Arab J Chem 2022;15:104105. https://doi.org/10.1016/j.arabjc.2022.104105.

[7] Monga D, Basu S. Novel MoS_2/C_3N_5 composites with extended spectral response towards highly efficient photocatalytic abatement of hazardous pollutants. J Environ Manage 2023;336:117570. https://doi.org/10.1016/j.jenvman.2023.117570.

[8] Jiang R, Lu G, Yan Z, Liu J, Wu D, Wang Y. Microplastic degradation by hydroxy-rich bismuth oxychloride. J Hazard Mater 2021;405:124247. https://doi.org/10.1016/j.jhazmat.2020.124247.

[9] Niu L, Zhang G, Xian G, Ren Z, Wei T, Li Q, et al. Tetracycline degradation by persulfate activated with magnetic γ-Fe_2O_3/CeO_2 catalyst: Performance, activation mechanism and degradation pathway. Sep Purif Technol 2021;259:118156. https://doi.org/10.1016/j.seppur.2020.118156.

[10] Monga D, Basu S. Enhanced photocatalytic degradation of industrial dye by g-C_3N_4/TiO_2 nanocomposite: Role of shape of TiO_2. Adv Powder Technol 2019;30:1089–98. https://doi.org/10.1016/j.apt.2019.03.004.

[11] Yang Q, Gao Y, Ke J, Show PL, Ge Y, Liu Y, et al. Antibiotics: An overview on the environmental occurrence, toxicity, degradation, and removal methods. Bioengineered 2021;12:7376–416. https://doi.org/10.1080/21655979.2021.1974657.

[12] Li S, Chen J, Hu S, Wang H, Jiang W, Chen X. Facile construction of novel Bi_2WO_6/Ta_3N_5 Z-scheme heterojunction nanofibers for efficient degradation of harmful pharmaceutical pollutants. Chem Eng J 2020;402:126165. https://doi.org/10.1016/j.cej.2020.126165.

[13] Dashairya L, Sharma S, Rathi A, Saha P, Basu S. Solar-light-driven photocatalysis by Sb_2S_3/carbon based composites towards degradation of noxious organic pollutants. Mater Chem Phys 2021;273:125120. https://doi.org/10.1016/j.matchemphys.2021.125120.

[14] Utami M, Wang S, Fajarwati FI, Salsabilla SN, Dewi TA, Fitri M. Enhanced Photodegradation of Rhodamine B Using Visible-Light Sensitive N-TiO_2/rGO Composite. Crystals 2023;13:588. https://doi.org/10.3390/cryst13040588.

[15] Goyal J, Sharma S, Basu S. Solar Light-Induced Photocatalytic Response of BiOCl/PANI Composite towards the Degradation of Tetracycline. Catalysts 2023;13:795. https://doi.org/10.3390/catal13050795.

[16] Amangelsin Y, Semenova Y, Dadar M, Aljofan M, Bjørklund G. The Impact of Tetracycline Pollution on the Aquatic Environment and Removal Strategies. Antibiotics 2023;12:440. https://doi.org/10.3390/antibiotics12030440.

[17] Fan B, Tan Y, Wang J, Zhang B, Peng Y, Yuan C, et al. Application of Magnetic Composites in Removal of Tetracycline through Adsorption and Advanced Oxidation Processes (AOPs): A Review. Processes 2021;9:1644. https://doi.org/10.3390/pr9091644.

[18] Leng Y, Xiao H, Li Z, Wang J. Tetracyclines, sulfonamides and quinolones and their corresponding resistance genes in coastal areas of Beibu Gulf, China. Sci Total Environ 2020;714:136899. https://doi.org/10.1016/j.scitotenv.2020.136899.

[19] Singla S, Devi P, Basu S. Highly Effectual Photocatalytic Remediation of Tetracycline under the Broad Spectrum of Sunlight by Novel $BiVO_4$/Sb_2S_3 Nanocomposite. Catalysts 2023;13:731. https://doi.org/10.3390/catal13040731.

[20] Sharma S, Basu S. Highly reusable visible light active hierarchical porous WO_3/SiO_2 monolith in centimeter length scale for enhanced photocatalytic degradation of toxic pollutants. Sep Purif Technol 2020;231:115916. https://doi.org/10.1016/j.seppur.2019.115916.

[21] Chankhanittha T, Nanan S. Visible-light-driven photocatalytic degradation of ofloxacin (OFL) antibiotic and Rhodamine B (RhB) dye by solvothermally grown ZnO/Bi_2MoO_6 heterojunction. J Colloid Interface Sci 2021;582:412–27. https://doi.org/10.1016/j.jcis.2020.08.061.

[22] Singla S, Sharma S, Basu S. MoS_2/WO_3 heterojunction with the intensified photocatalytic performance for decomposition of organic pollutants under the broad array of solar light. J Clean Prod 2021;324:129290. https://doi.org/10.1016/j.jclepro.2021.129290.

[23] Fan G, Ma Z, Li X, Deng L. Coupling of Bi_2O_3 nanoparticles with g-C_3N_4 for enhanced photocatalytic degradation of methylene blue. Ceram Int 2021;47:5758–66. https://doi.org/10.1016/j.ceramint.2020.10.162.

[24] Gupta G, Kaur M, Kansal SK, Umar A, Ibrahim AA. α-Bi_2O_3 nanosheets: An efficient material for sunlight-driven photocatalytic degradation of Rhodamine B. Ceram Int 2022;48:29580–8. https://doi.org/10.1016/j.ceramint.2022.06.210.

[25] Nagar A, Basu S. Fabrication of 3D porous peony flower-like -Bi_2O_3/BiOCl heterostructure for synergistically boosting the visible-light-driven degradation of organic pollutants. Environ Technol Innov 2021;24:101956. https://doi.org/10.1016/j.eti.2021.101956.

[26] Xu Z, Shi Y, Li L, Sun H, Amin MS, Guo F, et al. Fabrication of 2D/2D Z-scheme highly crystalline carbon nitride/δ-Bi_2O_3 heterojunction photocatalyst with enhanced photocatalytic degradation of tetracycline. J Alloys Compd 2022;895:162667. https://doi.org/10.1016/j.jallcom.2021.162667.

[27] Liu W, Li Z, Kang Q, Wen L. Efficient photocatalytic degradation of doxycycline by coupling α-Bi_2O_3/g-C_3N_4 composite and H2O2 under visible light. Environ Res 2021;197:110925. https://doi.org/10.1016/j.envres.2021.110925.

[28] Majhi D, Samal PK, Das K, Gouda SK, Bhoi YP, Mishra BG. α-NiS/Bi_2O_3 Nanocomposites for Enhanced Photocatalytic Degradation of Tramadol. ACS Appl Nano Mater 2019;2:395–407. https://doi.org/10.1021/acsanm.8b01974.

[29] Makhloufi R, Hachani SE, Fettah A, Tair W, Zekri Z. Synthesis of Sb_2S_3-$Sb_4O_5Cl_2$ composite used as a photocatalyst for crystal violet cationic dye degradation. Chem Data Collect 2022;39:100867. https://doi.org/10.1016/j.cdc.2022.100867.

[30] Ayappan C, Jayaraman V, Palanivel B, Pandikumar A, Mani A. Facile preparation of novel Sb_2S_3 nanoparticles/rod-like α-Ag_2WO_4 heterojunction photocatalysts: Continuous modulation of band structure towards the efficient removal of organic contaminants. Sep Purif Technol 2020;236:116302. https://doi.org/10.1016/j.seppur.2019.116302.

[31] Berekute AK, Yu K-P, Chuang Y-H, Lin K-Y. Novel visible-light-induced P-doped g-C_3N_4/α-Bi_2O_3 nanocomposite photocatalysts for enhanced degradation of refractory endocrine disruptors—benzophenones. Appl Surf Sci 2023;607:154987. https://doi.org/10.1016/j.apsusc.2022.154987.

[32] Kashmery HA, El-Hout SI. Bi_2S_3/Bi_2O_3 nanocomposites as effective photocatalysts for photocatalytic degradation of tetracycline under visible-light exposure. Opt Mater (Amst) 2023;135:113231. https://doi.org/10.1016/j.optmat.2022.113231.

[33] Subalakshmi A, Kavitha B, Srinivasan N, Rajarajan M, Suganthi A. An affordable efficient $SrWO_4$ decorated Bi_2O_3 nanocomposite: Photocatalytic activity for the degradation of methylene blue under visible light irradiation. Mater Today Proc 2022;48:409–19. https://doi.org/10.1016/j.matpr.2020.11.167.

[34] Pournemati K, Habibi-Yangjeh A, Khataee A. Ternary novel TiO_2/$MgBi_2O_6$/Bi_2O_3 nanocomposites with n-n-p heterojunctions: Impressive visible-light-triggered photocatalytic degradation of tetracycline. Adv Powder Technol 2022;33:103820. https://doi.org/10.1016/j.apt.2022.103820.

[35] Xiao Y, Wang H, Jiang Y, Zhang W, Zhang J, Wu X, et al. Hierarchical Sb_2S_3/$ZnIn_2S_4$ core–shell heterostructure for highly efficient photocatalytic hydrogen production and pollutant degradation. J Colloid Interface Sci 2022;623:109–23. https://doi.org/10.1016/j.jcis.2022.04.137.

[36] Li X, Yang K, Wang F, Shi K, Huang W, Lu K, et al. Constructing 0D/1D Bi_2S_3/Sb_2S_3 Z-scheme heterojunctions for efficient visible-light-driven degradation of dyes, Cr6+ reduction and H_2O_2 production. J Alloys Compd 2023;953:170064. https://doi.org/10.1016/j.jallcom.2023.170064.

[37] Dashairya L, Mehta A, Saha P, Basu S. Visible-light-induced enhanced photocatalytic degradation of Rhodamine-B dye using $Bi_xSb_{2-x}S_3$ solid-solution photocatalysts. J Colloid Interface Sci 2020;561:71–82. https://doi.org/10.1016/j.jcis.2019.11.118.

[38] Bouziani A, Yahya M, Bianchi CL, Falletta E, Celik G. Ternary Polyaniline@Bi_2O_3-BiOCl Nanocomposites as Innovative Highly Active Photocatalysts for the Removal of the Dye under Solar Light Irradiation. Nanomaterials 2023;13:713. https://doi.org/10.3390/nano13040713.

[39] Sharma S, Mehta SK, Ibhadon AO, Kansal SK. Fabrication of novel carbon quantum dots modified bismuth oxide (α-Bi_2O_3/C-dots): Material properties and catalytic applications. J Colloid Interface Sci 2019;533:227–37. https://doi.org/10.1016/j.jcis.2018.08.056.

[40] Shivanna S, Purushotham D, Kodandaram A, Nagabhushana CM, Mavinakere Ramesh A. Microwave assisted hydrothermal synthesis of Ag_2O/α-Bi_2O_3 heterostructures with highly

enhanced photocatalysis and their environmental interest. Chem Phys Impact 2023;6:100241. https://doi.org/10.1016/j.chphi.2023.100241.

[41] Wu C, Shen L, Huang Q, Zhang Y-C. Hydrothermal synthesis and characterization of Bi_2O_3 nanowires. Mater Lett 2011;65:1134–6. https://doi.org/10.1016/j.matlet.2011.01.021.

[42] Khalifeh MR, Shokrollahi H, Arab SM, Yang H. The role of Dy incorporation in the magnetic behavior and structural characterization of synthetic Ce, Bi-substituted yttrium iron garnet. Mater Chem Phys 2020;247:122838. https://doi.org/10.1016/j.matchemphys.2020.122838.

[43] Xian T, Sun X, Di L, Li H, Yang H. Improved photocatalytic degradation and reduction performance of Bi_2O_3 by the decoration of AuPt alloy nanoparticles. Opt Mater (Amst) 2021;111:110614. https://doi.org/10.1016/j.optmat.2020.110614.

[44] Torrisi L, Silipigni L, Cutroneo M, Torrisi A. Graphene oxide as a radiation sensitive material for XPS dosimetry. Vacuum 2020;173:109175. https://doi.org/10.1016/j.vacuum.2020.109175.

[45] Luo W, Ao X, Li Z, Lv L, Li J, Hong G, et al. Imbedding ultrafine Sb_2S_3 nanoparticles in mesoporous carbon sphere for high-performance lithium-ion battery. Electrochim Acta 2018;290:185–92. https://doi.org/10.1016/j.electacta.2018.09.070.

[46] Xu Q, Zheng C, Wang Z, Zhang Z, Su X, Sun B, et al. Synthesis of various morphologies of Sb_2S_3 based on amorphous-crystalline transition with related photodegradation. J Mater Sci 2022;57:7531–46. https://doi.org/10.1007/s10853-022-07135-6.

[47] Chen Y, Cheng Y, Zhao J, Zhang W, Gao J, Miao H, et al. Construction of Sb_2S_3/CdS/$CdIn_2S_4$ cascaded S-scheme heterojunction for improving photoelectrochemical performance. J Colloid Interface Sci 2022;627:1047–60. https://doi.org/10.1016/j.jcis.2022.07.117.

[48] Han T, Luo M, Liu Y, Lu C, Ge Y, Xue X, et al. Sb_2S_3/Sb_2Se_3 heterojunction for high-performance photodetection and hydrogen production. J Colloid Interface Sci 2022;628:886–95. https://doi.org/10.1016/j.jcis.2022.08.072.

[49] Gnanasekaran L, Hemamalini R, Rajendran S, Qin J, Yola ML, Atar N, et al. Nanosized Fe_3O_4 incorporated on a TiO_2 surface for the enhanced photocatalytic degradation of organic pollutants. J Mol Liq 2019;287:110967. https://doi.org/10.1016/j.molliq.2019.110967.

[50] Singla S, Basu S, Devi P. Solar light responsive 2D/2D $BiVO_4$/SnS_2 nanocomposite for photocatalytic elimination of recalcitrant antibiotics and photoelectrocatalytic water

splitting with high performance. J Ind Eng Chem 2023;118:119–31. https://doi.org/10.1016/j.jiec.2022.10.051.

[51] Zhao C, Guo J, Yu C, Zhang Z, Sun Z, Piao X. Fabrication of CNTs-Ag-TiO_2 ternary structure for enhancing visible light photocatalytic degradation of organic dye pollutant. Mater Chem Phys 2020;248:122873. https://doi.org/10.1016/j.matchemphys.2020.122873.

[52] Zhang R, Cai L, Cai Y, Han Q, Li Y, Zhang T, et al. Lamellar insert SnS_2 anchored on BiOBr for enhanced photocatalytic degradation of organic pollutant under visible-light. Colloids Surfaces A Physicochem Eng Asp 2021;618:126444. https://doi.org/10.1016/j.colsurfa.2021.126444.

[53] Kamranifar M, Allahresani A, Naghizadeh A. Synthesis and characterizations of a novel $CoFe_2O_4$@CuS magnetic nanocomposite and investigation of its efficiency for photocatalytic degradation of penicillin G antibiotic in simulated wastewater. J Hazard Mater 2019;366:545–55. https://doi.org/10.1016/j.jhazmat.2018.12.046.

[54] Aanchal, Barman S, Basu S. Complete removal of endocrine disrupting compound and toxic dye by visible light active porous g-C_3N_4/H-ZSM-5 nanocomposite. Chemosphere 2020;241:124981. https://doi.org/10.1016/j.chemosphere.2019.124981.

[55] Gao B, Lim TM, Subagio DP, Lim T-T. Zr-doped TiO_2 for enhanced photocatalytic degradation of bisphenol A. Appl Catal A Gen 2010;375:107–15. https://doi.org/10.1016/j.apcata.2009.12.025.

[56] Sharma S, Basu S. Construction of an efficient and durable hierarchical porous CuO/SiO_2 monolith for synergistically boosting the visible-light-driven degradation of organic pollutants. Sep Purif Technol 2021;279:119759. https://doi.org/10.1016/j.seppur.2021.119759.

[57] Monga D, Basu S. Combination of MoS_2 nanopetals with Ag nanoparticles decorated graphene oxide for boosting photocatalytic abatement of recalcitrant pollutants under visible light irradiation. Adv Powder Technol 2022;33:103555. https://doi.org/10.1016/j.apt.2022.103555.

[58] Dai W, Jiang L, Wang J, Pu Y, Zhu Y, Wang Y, et al. Efficient and stable photocatalytic degradation of tetracycline wastewater by 3D Polyaniline/Perylene diimide organic heterojunction under visible light irradiation. Chem Eng J 2020;397:125476. https://doi.org/10.1016/j.cej.2020.125476.

[59] Gupta D, Chauhan R, Kumar N, Singh V, Srivastava VC, Mohanty P, et al. Enhancing photocatalytic degradation of quinoline by ZnO:TiO_2 mixed oxide: Optimization of operating parameters and mechanistic study. J Environ Manage 2020;258:110032. https://doi.org/10.1016/j.jenvman.2019.110032.

[60] Li Z-Q, Chen X-T, Xue Z-L. Microwave-assisted synthesis and photocatalytic properties of flower-like Bi_2WO_6 and Bi_2O_3–Bi_2WO_6 composite. J Colloid Interface Sci 2013;394:69–77. https://doi.org/10.1016/j.jcis.2012.12.002.

[61] Yang H, Li M, Fu L, Tang A, Mann S. Controlled Assembly of Sb_2S_3 Nanoparticles on Silica/Polymer Nanotubes: Insights into the Nature of Hybrid Interfaces. Sci Rep 2013;3:1336. https://doi.org/10.1038/srep01336.

MSc Thesis

ORIGINALITY REPORT

15%	12%	12%	1%
SIMILARITY INDEX	INTERNET SOURCES	PUBLICATIONS	STUDENT PAPERS

PRIMARY SOURCES

1	www.mdpi.com Internet Source	4%
2	tudr.thapar.edu:8080 Internet Source	2%
3	Shelly Singla, Surbhi Sharma, Soumen Basu. "MoS2/WO3 heterojunction with the intensified photocatalytic performance for decomposition of organic pollutants under the broad array of solar light", Journal of Cleaner Production, 2021 Publication	2%
4	Shelly Singla, Pooja Devi, Soumen Basu. "Highly Effectual Photocatalytic Remediation of Tetracycline under the Broad Spectrum of Sunlight by Novel BiVO4/Sb2S3 Nanocomposite", Catalysts, 2023 Publication	1%
5	Shelly Singla, Soumen Basu, Pooja Devi. "Solar Light Responsive 2D/2D BiVO4/SnS2 Nanocomposite for Photocatalytic Elimination of Recalcitrant Antibiotics and	1%

	Photoelectrocatalytic Water Splitting with High Performance", Journal of Industrial and Engineering Chemistry, 2022 Publication	
6	pubs.rsc.org Internet Source	1%
7	www.researchgate.net Internet Source	<1%
8	idoc.pub Internet Source	<1%
9	aip.scitation.org Internet Source	<1%
10	Surbhi Sharma, Soumen Basu. "Visible-light-driven efficient photocatalytic abatement of recalcitrant pollutants by centimeter-length MoO3/SiO2 monoliths with long service life", Applied Materials Today, 2021 Publication	<1%
11	link.springer.com Internet Source	<1%
12	eprints.whiterose.ac.uk Internet Source	<1%
13	www.science.gov Internet Source	<1%
14	Chinnadurai Ayappan, Venkatesan Jayaraman, Baskaran Palanivel, Alagarsamy Pandikumar,	<1%

	Alagiri Mani. "Facile preparation of novel Sb2S3 nanoparticles/rod-like α-Ag2WO4 heterojunction photocatalysts: Continuous modulation of band structure towards the efficient removal of organic contaminants", Separation and Purification Technology, 2020 Publication	
15	Submitted to Aston University Student Paper	<1%
16	Submitted to Indian Institute of Technology Roorkee Student Paper	<1%
17	www.research-collection.ethz.ch Internet Source	<1%
18	Ferrandon, M.. "Copper Oxide-Platinum/Alumina Catalysts for Volatile Organic Compound and Carbon Monoxide Oxidation: Synergetic Effect of Cerium and Lanthanum", Journal of Catalysis, 20010910 Publication	<1%
19	repositorio.ipen.br Internet Source	<1%
20	Penuela, G.A.. "Application of C"1"8 disks followed by gas chromatography techniques to degradation kinetics, stability and monitoring of endosulfan in water", Journal of Chromatography A, 19980130 Publication	<1%

21	fr.scribd.com Internet Source	<1%
22	pureadmin.qub.ac.uk Internet Source	<1%
23	studentsrepo.um.edu.my Internet Source	<1%
24	www.frontiersin.org Internet Source	<1%
25	Love Dashairya, Akansha Mehta, Partha Saha, Soumen Basu. "Visible-light-induced enhanced photocatalytic degradation of Rhodamine-B dye using BixSb2-xS3 solid-solution photocatalysts", Journal of Colloid and Interface Science, 2020 Publication	<1%
26	Surbhi Sharma, Soumen Basu. "Fabrication of centimeter-sized Sb2S3/SiO2 monolithic mimosa pudica nanoflowers for remediation of hazardous pollutants from industrial wastewater", Journal of Cleaner Production, 2021 Publication	<1%
27	Submitted to Thapar University, Patiala Student Paper	<1%
28	www.bu.edu Internet Source	<1%

29	www.nrfhh.com Internet Source	<1%
30	Menglei Yuan, Junwu Chen, Yiling Bai, Zhanjun Liu, Jingxian Zhang, Tongkun Zhao, Qiaona Shi, Shuwei Li, Xi Wang, Guangjin Zhang. "Electrochemical C-N coupling with perovskite hybrids toward efficient urea synthesis", Chemical Science, 2021 Publication	<1%
31	cyberleninka.org Internet Source	<1%
32	ir.library.osaka-u.ac.jp Internet Source	<1%
33	www.jos.ac.cn Internet Source	<1%

Exclude quotes	On	Exclude matches	< 8 words
Exclude bibliography	On